JOURNAL OF COMPUTATIONAL PHYSICS 72, 78–120 (1978)

Errors for Calculations of Strong Shocks Using an Artificial Viscosity and an Artificial Heat Flux*

W. F. NOH

Lawrence Livermore National Laboratory,
P.O. Box 808, University of California, Livermore, California 94550

Received June 2, 1986; revised October 15, 1986

The artificial viscosity (Q) method of von Neumann and Richtmyer is a tremendously useful numerical technique for following shocks wherever and whenever they appear in the flow. We show that it must be used with some caution, however, as serious Q-induced errors (on the order of 100%) can occur in some strong shock calculations. We investigate three types of Q errors: 1. Excess Q heating, of which there are two types: (a) excess wall heating on shock formation and (b) shockless Q heating; 2. Q errors when shocks are propagated over a nonuniform mesh; and 3. Q errors in propagating shocks in spherical geometry. As a basis of comparison, we use as our standard the Lagrangian formulation with $Q = C_0^2 \rho l^2 (u_x)^2$. This standard Q is compared with Noh's (Q & H) shock-following method, which employs an artificial heat flux (H) in addition to Q, and with the (non-Q) piecewise-parabolic method (PPM) of Colella and Woodward. Both the (Q & H) method and PPM (particularly when used with an adaptive shock-tracking mesh) give superior results for our test problems. In spherical geometry, Schulz's and Whalen's tensor Q formulations of the hydrodynamic equations prove to be more accurate than the standard Q formulation, and when Schulz's formulation is combined with Noh's (Q & H) method, superior results are achieved.

1. INTRODUCTION

The artificial viscosity (Q) method of von Neumann and Richtmyer [1] is a tremendously useful numerical technique for following shocks wherever and whenever they appear in the flow. However, as we shall see, it must be used with some caution, as serious Q-induced errors can occur in some calculations of strong shocks.

We investigate three types of Q errors:

1. Excess Q heating, of which there are two types: (a) excess **wall heating** on shock formation and (b) **shockless Q heating**;
2. Q errors when shocks are propagated over a **nonuniform mesh**; and
3. Q errors in propagating shocks in **spherical geometry**.

We use, as a basis of comparison, the Lagrangian formulation of the hydrodynamic equations given in Ref. 1, with the **standard** $Q = C_0^2 \rho l^2 (u_x)^2$. In Sec-

* This work was performed under the auspices of the United States Department of Energy by the Lawrence Livermore National Laboratory under Contract W-7405-ENG-48.

0021-9991/87 $3.00

tion 2, the Lagrangian differential equations with Q (in plane ($\delta = 1$), cylindrical ($\delta = 2$), and spherical ($\delta = 3$) geometry) are given, and we include an artifical heat flux $H = h_0^2 \rho l^2 |u_x| \varepsilon_x$ used in Noh's (Q & H) shock-following method [2].[1] For our comparisons, three Q's are defined: Q_L, $Q_L(v)$, and Q_E. Q_L (the **standard** Q above) and Q_L(v) (the original Q of [1]) are referred to as Lagrangian (L) formulations, in that they spread shocks over a fixed number of (Lagrange) mesh intervals ($\simeq 3$), independent of their actual physical size, while Q_E is referred to as an Eulerian, or fixed-length formulation of Q, which spreads shocks over a fixed physical (Eulerian) distance ($\simeq 3\Delta x_{max}$). Only $Q_L(v)$ depends on the geometry δ (see [3, p. 319]), and as we show later, this dependence on δ introduces the most **shockless** Q **heating** error of any Q and the most Q error for shocks in spherical geometry. Thus, $Q_L(v)$ is not a preferred choice. We also define two H's, H_L and H_E, where H_L is used in conjuncton with Q_L, and H_E is used with Q_E in the (Q & H) method.

In Section 3, we give the difference equations and formulations of the Q's and H's. The **nominal** difference formulation of Q_L is $Q_L = 2\rho(\Delta u)^2$, in which the l of the **standard** Q is taken to be equal to the Lagrange interval (Δx), and the coefficient $C_0^2 = 2$. This is the **benchmark** Q used in our comparisons. We refer to this use of Q_L as the **standard calculation**.

There are two excess Q heating errors: (1) excess wall (or piston) heating due to Q, which occurs on shock formation (e.g., at a rigid wall where a gas is brought to rest and a shock is propagated away, or at the sudden startup of a piston) and (2) Q heating for shockless compressions (i.e., when $u_r < 0$ and no shock is present).

In Section 4, we investigate the wall heating Q error in test problem 1. This is an infinite-stength, constant-velocity shock in a perfect ($\gamma = \frac{5}{3}$) gas. A cold gas ($\varepsilon^0 = P^0 = 0$), initially moving with velocity $u^0 = -1$, is brought to rest by a rigid wall located at the origin. A shock is generated at the rigid wall and moves to the right with constant states ($u^+ = 0$, $\rho^+ = 4$, $\varepsilon^+ = 0.5$, etc.) and a constant shock speed ($S = \frac{1}{3}$).

The excess wall heating error occurs in the first few zones near the wall and shows up as overheating, or what is equivalent, a dip in the density (Fig. 1). (That is, since the post-shock pressure P^+ is nearly constant, then, for $P^+ = (\gamma - 1)\rho^+\varepsilon^+$, a peak in ε^+ results in a dip in ρ^+.) This error goes with the size of the Q coefficients, C_0^2 and C_1 (Fig. 2), and is also seen to depend on the Q formulation (Fig. 3). That is, in Fig. 3, we see that the error is larger for Q_E than for Q_L (with the same size coefficients C_0^2 and C_1). By numerical arguments (Section 4.2), and from Fig. 4, we see that this Q error is inevitable and is, in fact, built into the **exact solution** of the **differential equations** (2.1) with Q given by (2.2). Indeed, we argue (Section 4.2) that such a wall heating error will occur for any shock-smearing method (in the absence of heat conduction), whether a viscosity Q occurs explicitly in the method or not. Now, because the **(Q & H) shock-following method** does

[1] The idea behind the (Q & H) shock-following method is to approximate nature more closely by smearing shock discontinuities using artificial heat conduction as well as artificial viscosity. In particular, hot spots caused by using Q alone are eliminated, or at least reduced by using both Q and H.

include an (artificial) heat-conduction term H, then, as in nature, the excess wall heating error is eliminated. This is seen by comparing Fig. 5 (no heat conduction) with Fig. 6 using the same Q as in Fig. 5, but with the heat flux $H \neq 0$, and indeed the wall heating error has been eliminated.

In Section 5, we investigate the **shockless Q heating** error using a class of test problems (with exact solutions for all geometries δ) called **uniform collapse** [5]. Here, the fluid is shockless, even though it is everywhere compressing. In the Q method, an energy error, $\Delta\varepsilon$, occurs for Q_L, Q_E, and for $Q_L(v)$. In particular, in spherical geometry ($\delta = 3$), the $Q_L(v)$ energy error, $\Delta\varepsilon_L(v)$, is nine times as large as the Q_L energy error, $\Delta\varepsilon_L$ (i.e., $\Delta\varepsilon_L(v) = \delta^2 \Delta\varepsilon_L = 9\Delta\varepsilon_L$). This fact strongly rules in favor of our use of $Q_L = 2\rho(\Delta u)^2$ as the **standard** Lagrange formulation of Q, rather than the original $Q_L(v)$ suggested in Ref. 1.

In Section 6, we investigate the **second type** of Q error by introducing a nonuniform mesh ($\Delta x_{k+1} = R\Delta x_k$, where R is a constant) into problem 1 (see Fig. 7). As our **standard** Q, we use $Q_L = 2\rho(\Delta u)^2$ and compare the Q_L errors for $R = 1.05$, 1.15, and 1.25 in Figs. 8, 9, and 10. Because the type 2 errors approach 100%, they can be a serious concern. A remedy is to use Q_E, the fixed-length Q (Fig. 11). Here we see that Q_E completely eliminates this nonuniform mesh error, but that the wall heating error is very large. By using both Q_E and H_E in the (Q_E & H_E) method (Fig. 12), we see that **all error** is eliminated. That is, the (Q_E & H_E) shock-following method offers a 100% fix for both the type 1 and type 2 errors.

Unfortunately, using Q_E spreads shocks over a fixed physical distance of $\simeq 3\Delta x_{max}$, which is unacceptable in those regions of the problem where a smaller mesh interval occurs. Now this nonuniform mesh error clearly depends on the Q formulation, and we can ask, "Is it possible to find a Lagrange (L) formulation of Q (i.e., where $l = \Delta x$) for which this type of error is also zero?" The answer appears to be that this is unlikely, because comparisons of other Q_L's [6] (see Fig. 13) show a comparable error for all of the Q_L's tested.

Section 7 contains a theoretical explanation for the errors associated with letting $l = \Delta x$ in Q_L. This implies that l depends on x [i.e., $l = l(x)$] in the **differential** formulation of Q_L, which, in turn, leads to a fictitious frame-of-reference velocity in the **differential equations**. This fictitious frame of reference is then shown to account for the observed errors. As a result, this error (due to letting $l = l(x)$) can be expected in all Lagrangian formulations. The fact that this error is already an error in the solution of the **differential equations** is established numerically in Fig. 14.

As we note in Fig. 13, the nonuniform mesh error increases with C_0^2 and C_1, and thus we would like to minimize C_2^2 and C_1. In particular, the (Q_L & H_L) method permits us to use considerably smaller Q_L coefficients, while at the same time eliminating the type 1 wall heating error. This can be seen in Figs. 15 and 16, where indeed the wall heating error is eliminated altogether, and we note that using H_L with Q_L results in smoother shocks. Having smoother shocks permits us to reduce the Q_L constants. In Fig. 16, when we take $C_0^2 = 1$ and $C_1 = 0$, we see that this choice minimizes the type 2 error. The (Q_L & H_L) method thus is an acceptable procedure if the unequal zoning is not too severe.

In Section 8, we investigate the spherical-geometry Q errors using Noh's spherical-shock test problem [2] (Fig. 17), which for $\delta = 3$ is just a generalization of test problem 1. This type 3 error is considerably more complicated than the previous Q errors, in that it depends both on the Q formulation [e.g., Q_L vs $Q_L(v)$], and also as to whether Q is treated as a scalar viscosity as in Ref. 1 or as a tensor viscosity, as given by Schulz [8] or Whalen [9]. That the errors are truly enormous is seen in Fig. 18, where the error for the **standard** Q_L formulation is nearly 600% near the origin and nearly 1000% for $Q_L(v)$—the original definition of Q (when generalized to spherical geometry) given in Ref. 1. In Fig. 19, we see just how serious this error can be and how slowly the solution converges to the exact solution (i.e., $\rho^+ = 64$). Indeed, even for 800 mesh points in the unit sphere ($K = 800$), there is still a considerable error near the origin.

The explanation is given in Fig. 20, where we show that the error results from the finite shock thickness, which prevents the Q method from determining the correct preshock density. (That is, the shock spreading picks $\rho^- < \rho^-_{\text{exact}} = 16$). In Fig. 21 we argue numerically (as in Section 4) that this type 3 error is already in the **exact solution** of the **differential equations with** Q (and is thus not related to any particular difference method). Indeed, the error is due entirely to the finite shock thickness. We conclude that sharper shocks give smaller Q errors. This is shown in Fig. 22, where the Q_L and $(Q_L \,\&\, H_L)$ methods are compared. The $(Q_L \,\&\, H_L)$ solution gives both smoother and more accurate results, and indeed, Fig. 22b shows the internal energy using (Q & H) to be essentially correct (i.e., $\varepsilon^+ = \frac{1}{2}$).

By comparing various Q_L's and $(Q_L \,\&\, H_L)$ in Fig. 23, it is clear that sharper shocks produce less error. The (non-Q) PPM of Colella and Woodward [7] produces even sharper shocks (Fig. 24) than any of the Q methods (i.e., PPM spreads shocks over only one or two mesh intervals), and thus, for the 100-zone unit-sphere test problem, PPM is superior to all of the scalar (S) Q_L or $(Q_L \,\&\, H_L)$ methods shown in Fig. 23. The small error in PPM is further reduced by using an adaptive mesh technique to capture the shock. The results (Fig. 24) show that using 400 zones (with an adaptive mesh) is equivalent to a 1200-zone (essentially converged) normal PPM problem.

Section 9 contains Schulz's tensor Q formulation (T) of the hydrodynamic equations, along with his artificial viscosity, Q_L(S), definition [8]. The calculations using this tensor formulation (Fig. 25) show a significant improvement over the standard scalar (S) solutions (e.g., Fig. 23). However, only a slight improvement is obtained using Schulz's Q_L(S) over the **standard** Q_L, and we conclude that it is the tensor equations (T) that are important, and not so much which Q_L formulation is used. In Fig. 26, the (T) formulations for Q_L (T) and $(Q_L \,\&\, H_L)$ (T) are compared. Figure 26b shows that the energy error is almost zero using the $(Q_L \,\&\, H_L)$ (T) method. Again, sharper shocks reduce this type 3 error, and nearly exact results are achieved using a very small Q_L constant ($C_0^2 = \frac{1}{4}$) and by employing the $(Q_L \,\&\, H_L)$ (T) method ($Q_L = (\frac{1}{4})(\Delta u)^2$ and $H_L = 10\rho\,|\Delta u|\,\Delta\varepsilon$, Figs. 27a and b). In Fig. 28, the various Q_L's, $(Q_L \,\&\, H_L)$ methods, and (non-Q) PPM are compared. The best results [in the standard 100-zone ($K = 100$) problem are obtained using the tensor

formulation of the (Q_L & H_L) method with a small Q_L coefficient C_0^2. The best overall results are obtained with the (non-Q) PPM using an adaptive-mesh shock-following procedure, where, however, one should note that 400 mesh points are used in the shock-capturing procedure vs 100 mesh points for the other methods. The point to be emphasized here is that adaptive-mesh procedures can define shocks very accurately and are suggested for all shock-following methods.

Section 10 contains Whalen's [9] tensor formulation of the hydrodynamic equations and his definition Q_L^R of a tensor Q. His results, shown in Figs. 29 and 30, are remarkably accurate, even for a mesh as coarse as $K=25$ (Fig. 30). It is not yet clear whether his tensor formulation gives equally good results for more complicated shock problems, and we await further word on this from Whalen. Clearly, though, his formulation, (10.6) and (10.7), produces the most accurate (Q only) results for our test problem and needs to be investigated further.

In Section 11, we conclude that the Q errors of types 1, 2, and 3 are not due to the difference-method solution, and thus our difference equations do not contribute to the Q errors that we investigate. Rather, Q errors are intrinsic to the artificial viscosity (Q) shock-following method itself, and are thus already contained in the exact solution to the **differential equations with** Q. Consequently, improvements must be sought to modify the Q method (e.g., by using a tensor formulation and using both Q and H to follow shocks) or to minimize the physical shock thickness, as in the non-Q PPM, or more generally by using an adaptive-mesh shock-capturing procedure. In all cases, narrow shocks produce the least error.

2. Lagrangian Fluid Equations with Artificial Viscosity Q and Heat Flux H

Von Neumann and Richtmeyer [1] considered their artificial viscosity Q to be a scalar quantity, and we take their formulation of the Lagrangian fluid equations as our standard. Also, the new (Q & H) shock-following method of Noh [2] (which uses an artificial heat-flux H in addition to the artificial-viscosity Q to follow shocks) is included in the formulation.

2.1. *Differential Equations*

The independent Lagrange variables are r and t, where r is taken as the initial position of the Eulerian (physical) coordinate (i.e., $R(r, 0)=r$); and u, ρ, ε, P, Q, and H are the velocity, density, internal energy, pressure, artificial viscosity [1], and artificial heat flux [2], respectively. A more useful independent variable is the mass, m, where, by the conservation of mass, we can write $dm=\delta\rho R^{\delta-1}\,dR=\delta\rho^0 r^{\delta-1}\,dr=\rho^0\,dr^\delta$, and the differential equations for plane ($\delta=1$), cylindrical ($\delta=2$), and spherical ($\delta=3$) geometries are as follows (with the usual notation $\partial f/\partial t=f_t$, $\partial f/\partial r=f_r$, $\partial f/\partial m=f_m$, etc.):

$$
\begin{aligned}
u_t &= -\delta R^{\delta-1}(P+Q)_m && \text{momentum} \\
R_t &= u && \text{position} \\
v &= (1/\rho) = (R^\delta)_m && \text{mass} \\
\varepsilon_t &= -(P+Q)v_t + \delta(R^{\delta-1}H)_m && \text{energy} \\
P &= P(\rho, \varepsilon) && \text{equation of state}
\end{aligned} \tag{2.1}
$$

and where Q and H are to be specified.

2.2. *Definitions of Q and H*

We include linear terms in Q and H [2, 5]. These are used in some of the Q error comparisons to produce smoother shock profiles, but otherwise do not affect the Q errors that we consider. The subscripts L and E refer to whether the space derivatives are in terms of the Lagrangian independent variable, r, or in terms of the Eulerian (physical) space coordinate, R:

Standard Lagrange Q:

$$
Q_{\mathrm{L}}(C_0^2, C_1) = \begin{cases} C_0^2 \rho l^2 (u_r)^2 - C_1 \rho C_s l u_r, & \text{if } u_r < 0, \\ 0, & \text{if } u_r \geqslant 0; \end{cases} \tag{2.2}
$$

Standard Lagrange H:

$$
H_{\mathrm{L}}(h_0^2, h_1) = \begin{cases} h_0^2 \rho l^2 \, |u_r| \, \varepsilon_r + h_1 \rho C_s l \varepsilon_r, & \text{if } Q_{\mathrm{L}} \neq 0, \\ 0, & \text{if } Q_{\mathrm{L}} = 0; \end{cases} \tag{2.3}
$$

Eulerian (fixed-length) Q:

$$
Q_{\mathrm{E}}(C_0^2, C_1) = \begin{cases} C_0^2 \rho l^2 (u_R)^2 - C_1 \rho C_s l u_R, & \text{if } u_R < 0, \\ 0, & \text{if } u_R \geqslant 0; \end{cases} \tag{2.4}
$$

Eulerian (fixed-length) H:

$$
H_{\mathrm{E}}(h_0^2, h_1) = \begin{cases} h_0^2 \rho l^2 \, |u_R| \, \varepsilon_R + h_1 \rho C_s l \varepsilon_R, & \text{if } Q_{\mathrm{E}} \neq 0, \\ 0, & \text{if } Q_{\mathrm{E}} = 0; \end{cases} \tag{2.5}
$$

Original Lagrange Q [1]:

$$
Q_{\mathrm{L}}(v) = \begin{cases} (C_0 \rho^0 l)^2 \rho (r/R)^{2\delta-2} (v_t)^2, & \text{if } v_t < 0, \\ 0, & \text{if } v_t \geqslant 0; \end{cases} \tag{2.6}
$$

where C_0, C_1, h_0, and h_1 are dimensionless constants; l is a constant with the dimensions of length and is related to the shock width ($\simeq 3l$); C_s is the local speed of sound; and in (2.6), $\rho^o = \rho(r, o)$ is the initial density.

We note that the Lagrangian and Eulerian formulations, Q_L and Q_E, and H_L and H_E are related by the **Jacobian** $J = R_r$, where for the quadratic terms (i.e., setting $C_1 = 0$ and $h_1 = 0$)

$$Q_L = R_r^2 Q_E \qquad \text{and} \qquad H_L = R_r^2 H_E,$$

or, in general,

$$Q_L(C_0^2, C_1) = Q_E[(C_0 R_r)^2, C_1 R_r]$$

and

$$H_L(h_0^2, h_1) = H_E[(h_0 R_r)^2, h_1 R_r].$$

Equation (2.6) is the original von Neumann–Richtmyer Q formulation expressed in terms of the specific volume, $v = (1/\rho)$, and is the only Q here to depend on the geometry (δ) (see also [3, p. 319]). In particular, both (2.2) (with $C_1 = 0$) and (2.6) are identical for plane geometry ($\delta = 1$). That is, from (2.1) and $\delta = 1$, $v_t = R_{mt} = R_{tm} = u_m = (1/\rho^o)u_r$ from which it follows that (2.6) reduces to (2.2). This also points out that (2.6) is indeed a Lagrange (L) formulation of Q.

In the Lagrange formulation (L), the *standard use* is to take $l = \Delta r$, which spreads shocks over a *fixed number* ($\simeq 3$) of mesh intervals (ΔR) (regardless of their size). In the Eulerian (fixed-length) formulation (E), shocks are spread over a *fixed* (physical) *length* ($\simeq 3l$), again independent of mesh size. Hence in the Eulerian formulation, one must take $l \simeq \Delta R_{\max} \geqslant \Delta r_{\max}$. That is, to define a shock numerically, it must be spread over at least two or three mesh intervals (ΔR), and thus for Q_E, we should take $l \simeq \Delta R_{\max}$; but it generally suffices to let $l \simeq \Delta r_{\max} = \Delta R^0_{\max}$, and we do this for our problems.

The usage, when H is included, is to take Q_L and H_L together and H_E with Q_E. These are referred to as the (Q & H) **shock-following method**.

3. Difference Equations

Here we essentially follow the staggered mesh (in time and space) difference formulation of the fluid equations given by von Neumann–Richtmyer [1]; however, we deviate slightly from their formulation to ensure that total energy is conserved.[2] These equations have proven to be very accurate over the years, and indeed, we conclude that they are very accurate for our study of strong shock errors.

[2] A final pressure $P^{n+1} = P(\rho^{n+1}, \varepsilon^{n+1})$ is available; however, it is not compted. This is done so that the total energy defined (in the sense of Trigger and Trulio [4]) as $\varepsilon^{n+1} = (\frac{1}{2})u^{n+3/2}u^{n+1/2} + \varepsilon^{n+1}$ is conserved. This is ensured if the final pressure is indeed given by (3.5), and ε^{n+1} by (3.6). (In Ref. 1, $\bar{P}^{n+1} + \bar{P}^n$ of (3.6) is taken to be $P^{n+1} + P^n + 2Q^{n+1/2}$, i.e., only the latest Q is used in the energy equation; and in Ref. 4, this choice is shown not to conserve total energy.)

3.1. *Difference Equations for Plane, Cylinder, and Sphere* ($\delta = 1, 2, 3$)

Let $\bar{P}^n = P^n + Q^{n-1/2}$, $(\Delta\bar{P})^n_k = \bar{P}^n_{k+1/2} - \bar{P}^n_{k-1/2}$, $\Delta m_{k+1/2} = \rho^0_{k+1/2}(r^\delta_{k+1} - r^\delta_k)$, and $\Delta m_k = \frac{1}{2}(\Delta m_{k+1/2} + \Delta m_{k-1/2})$, etc. Then (for **constant** Δt),

$$u^{n+1/2}_k = u^{n-1/2}_k - \frac{\delta\,\Delta t}{\Delta m_k}(R^n_k)^{\delta-1}(\Delta\bar{P})^n_k, \tag{3.1}$$

$$R^{n+1}_k = R^n_k + \Delta t\, u^{n+1/2}_k, \tag{3.2}$$

$$v^{n+1}_{k+1/2} = \left[\frac{\Delta(R^\delta)}{\Delta m}\right]^{n+1}_{k+1/2}; \tag{3.3}$$

and the energy ε is evaluated in two passes (see footnote 2) (with all subscripts at $k+\frac{1}{2}$);

$$\tilde{\varepsilon}^{n+1} = \varepsilon^n - \bar{P}^n(v^{n+1} - v^n) + \frac{\delta\,\Delta t}{\Delta m}\Delta(R^{\delta-1}H)^n, \tag{3.4}$$

$$P^{n+1} = P(\rho^{n+1}, \tilde{\varepsilon}^{n+1}), \tag{3.5}$$

$$\varepsilon^{n+1} = \varepsilon^n - \frac{(\bar{P}^{n+1} + \bar{P}^n)}{2}(v^{n+1} - v^n) + \frac{\delta\,\Delta t}{\Delta m}\frac{\Delta[(R^{\delta-1}H)^n + (R^{\delta-1}\tilde{H})^{n+1}]}{2}, \tag{3.6}$$

where $\tilde{H}^{n+1} = H[\rho^{n+1/2}, u^{n+1/2}, \tilde{\varepsilon}^{n+1}]$.

3.2. *Difference Definitions of Q and H*

We restrict our definitions to the quadratic terms (i.e., set $C_1 = h_1 = 0$), since the linear terms follow similarly. Let

$$(\Delta r)_{k+1/2} = r_{k+1} - r_k, \qquad (\Delta R)_{k+1/2} = R_{k+1} - R_k, \qquad (\Delta u)_{k+1/2} = u_{k+1} - u_k,$$

and define

$$(\Delta\bar{u})^{n+1/2}_{k+1/2} = \begin{cases} (\Delta u)^{n+1/2}_{k+1/2} & \text{if } (\Delta u)^{n+1/2}_{k+1/2} < 0, \\ 0 & \text{if } (\Delta u)^{n+1/2}_{k+1/2} \geqslant 0, \end{cases} \tag{3.7}$$

then the difference formulations are given by

$$\textbf{Standard Q:} \quad (Q_L)^{n+1/2}_{k+1/2} = C_0^2[\rho(\Delta\bar{u})^2]^{n+1/2}_{k+1/2}, \tag{3.8}$$

which is obtained by taking $l = \Delta r$ in (2.2) and likewise in (2.3) to obtain the

$$\textbf{Standard H:} \quad (H_L)^n_k = 2h_0^2\left[\frac{(\rho\,|\Delta\bar{u}|)^{n+1/2}_{k+1/2}\cdot(\rho\,|\Delta\bar{u}|)^{n+1/2}_{k-1/2}}{(\rho\,|\Delta\bar{u}|)^{n+1/2}_{k+1/2} + (\rho\,|\Delta\bar{u}|)^{n+1/2}_{k-1/2}}\right](\varepsilon^n_{k+1/2} - \varepsilon^n_{k-1/2}), \tag{3.9}$$

$$\textbf{Fixed-length Q:} \quad (Q_E)^{n+1/2}_{k+1/2} = (C_0 l)^2\left[\rho\left(\frac{\Delta\bar{u}}{\Delta R}\right)^2\right]^{n+1/2}_{k+1/2}, \tag{3.10}$$

and

$$(H_E)_k^n = 4(h_0 l)^2 \left[\frac{\left(\rho\left|\frac{\Delta\bar{u}}{\Delta R}\right|\right)_{k+1/2}^{n+1/2} \cdot \left(\rho\left|\frac{\Delta\bar{u}}{\Delta R}\right|\right)_{k-1/2}^{n+1/2}}{\left(\rho\left|\frac{\Delta\bar{u}}{\Delta R}\right|\right)_{k+1/2}^{n+1/2} + \left(\rho\left|\frac{\Delta\bar{u}}{\Delta R}\right|\right)_{k+1/2}^{n+1/2}} \right] \left[\frac{\varepsilon_{k+1/2}^n - \varepsilon_{k-1/2}^n}{R_{k+1}^{n+1} - R_{k-1}^{n+1}} \right], \tag{3.11}$$

the **fixed-length H**.

In (3.10) and (3.11), l is taken to be (a constant) $l = (\Delta R_{k+1/2}^0)_{\max}$, and shocks will then be spread over a length ($\simeq 3l$). The **original von Neumann–Richtmyer** [1] $Q_L(v)$ of (2.6) is given by

$$[Q_L(v)]_{k+1/2}^{n+1/2} = (C_0\rho^0)^2(\Delta r)_{k+1/2}^2 \rho_{k+1/2}^{n+1/2} \left(\frac{r}{R^{n+1}}\right)_{k+1/2}^{2\delta-2} \left(\frac{v_{k+1/2}^{n+1} - v_{k+1/2}^n}{\Delta t}\right)^2 \tag{3.12}$$

if $\Delta v/\Delta t < 0$, otherwise 0. Or, in divergence form, (i.e., (2.6) can also be expressed as $Q_L(v) = C_0^2\rho(lR_r)^2[u_R + (\delta-1)u/R]^2$); taking $l = \Delta r$,

$$[Q_L(v)]_{k+1/2}^{n+1/2} = C_0^2 \rho_{k+1/2}^{n+1/2} \left[\Delta u + \frac{(\delta-1)\, u\, \Delta R}{R}\right]_{k+1/2}^{n+1/2},$$

$$\text{if } \frac{\Delta v}{\Delta t} < 0, \text{ otherwise 0.} \tag{3.13}$$

We also note that, of the Q's and H's, only $Q_L(v)$ depends on the geometry δ.

We will abbreviate (3.8) to $Q_L(C_0^2) = C_0^2\rho(\Delta u)^2$ or, more generally,

$$Q_L(C_0^2, C_1) = C_0^2\rho(\Delta u)^2 - C_1\rho C_s(\Delta u) \tag{3.14}$$

in the test calculations. Likewise for $H_L(h_0^2, h_1)$, etc. The nominal value for C_0^2 is taken to be 2; so that our **standard calculations** will be denoted by

$$Q_L(2) = 2\rho(\Delta u)^2. \tag{3.15}$$

4. Excess Q Heating Errors

4.1. *The Wall Heating Error Test Problem*

Test problem 1 is that of a constant-state, constant-velocity shock of infinite strength (i.e., the preshock pressure $P^- = P^0 = 0$). The shock is generated in a perfect ($\gamma = \frac{5}{3}$) gas by bringing the cold ($\varepsilon^0 = 0$) gas to rest at a rigid wall. This is just the familiar constant-velocity, piston-driven shock, but in a frame of reference where the piston (here a rigid wall at $x = 0$) is at rest. The particular initial conditons chosen are $u^0 = -1$, $\rho^0 = 1$, $\varepsilon^0 = 0$, and thus $P^0 = (\gamma - 1)\,\rho^0\varepsilon^0 = 0$. The post-shock solution is $u^+ = 0$, $\rho^+ = 4$, $\varepsilon^+ = \frac{1}{2}$, and $P^+ = \frac{4}{3}$ (see Fig. 17b, $\delta = 1$). In Fig. 1,

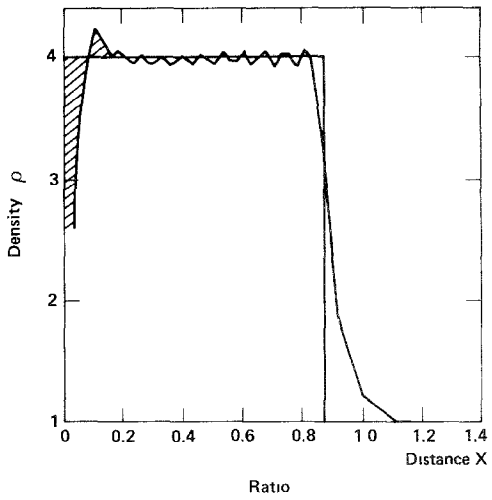

FIG. 1. The **standard calculation**, where $Q_L = 2\rho(\Delta u)^2$. The shaded area is the error in density due to the type 1 wall heating error. That is, $P^+ = (2/3)\rho^+\varepsilon^+$, and for this problem, P^+ **is correct**; therefore, the density error in ρ^+ is inversely related to the error in ε^+. In other words, a too-large value of ε^+ implies that ρ^+ implies that ρ^+ is too small.

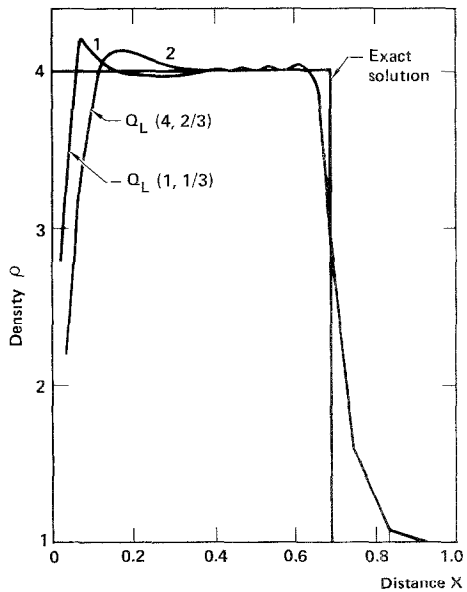

FIG. 2. When we compare curve 1, $Q_L(1, \frac{1}{3}) = \rho(\Delta u)^2 - \frac{1}{3}\rho C_S(\Delta u)$, and curve 2, $Q_L(4, \frac{2}{3}) = 4\rho(\Delta u)^2 - \frac{2}{3}\rho C_S(\Delta u)$, with the exact solution, we see that the wall heating Q error increases with the magnitude of the Q_L constants C_0^2 and C_1.

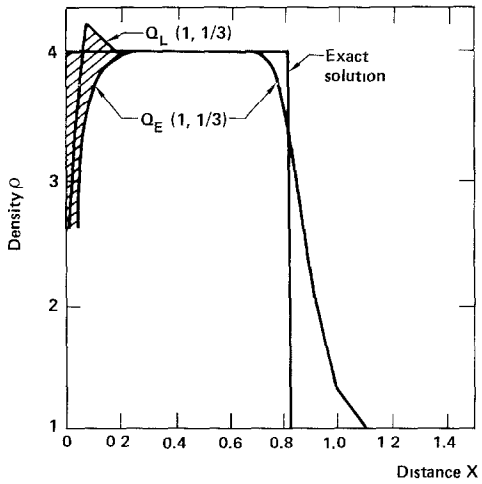

FIG. 3. The wall heating error (shaded regions) is larger for Q_E than for Q_L with the same size coefficients C_0^2 and C_1. Thus, this error also depends on the Q formulation to some extent.

ρ^+ is plotted for our **standard calculation** using $Q_L(2) = 2\rho(\Delta u)^2$. The wall heating error (the shaded area) occurs typically in the first three zones next to the wall (or piston).

Figure 2 shows the dependence of the wall heating error on the magnitude of C_0^2 and C_1. Here, $Q_L(1, \frac{1}{3})$ is compared with $Q_L(4, \frac{2}{3})$ (i.e., $C_0^2 \to (2C_0)^2$, and $C_1 \to 2C_1$) and the exact solution. Clearly, the $\Delta\rho_\rho^+$ error increases with C_0^2 and C_1. Consequently, the smaller the coefficient C_0^2 (and C_1) the better,[3] and as we shall see later, all of the Q errors that we investigate increase with C_0^2 (and C_1).

Figure 3 is a comparison of ρ_L^+ with ρ_E^+ for Q_L and Q_E (with $C_0^2 = 1$ and $C_1 = \frac{1}{3}$ for both Q's). The error $\Delta\rho_E^+ = \rho_{\text{exact}}^+ - \rho_E^+ = 4 - \rho_E^+$ is seen to be considerably greater than the error $\Delta\rho_L^+$. This shows that the wall heating error depends to some extent on the Q formulation; however, it cannot be eliminated by some new definition of Q, since (as we shall show below) all shock-smearing methods, inevitably, have some wall heating error.

4.2. *Theoretical Discussion*

We want to demonstrate that the wall heating Q error is unavoidable and is already an error in the solution of the **differential equations** with Q. The proof is numerical in that we seek convergence using mesh refinement. We consider Q_L of (2.2) as typical. We want to **hold l fixed** in (2.2) and seek convergence to the **exact** solution by letting $\Delta r \to 0$. We can do this most simply by noting first that the effect

[3] In particular, a noisier shock results from the use of a smaller C_0^2 (and C_1), but this noise does not seem, in practice, to result in any numerical error. Thus, a noisier shock is to be preferred (even though a smooth shock is esthetically more appealing). We note later that one of the main advantages of the (Q & H) shock-following method is that shocks are much smoother when a heat flux H is used in addition to Q, and thus one can use even smaller constants C_0^2 and C_1.

on Q of decreasing Δr (while holding l constant) is simply equivalent to increasing C_0 and C_1 in (3.8). For example, letting $\Delta r \to \Delta r/2$ (and letting $\Delta t \to \Delta t/2$—which maintains stability in the difference equations) is equivalent to just doubling the Q_L constants C_0 and C_1(i.e., letting $C_0 \to 2C_0$ and $C_1 \to 2C_1$). Second, in the remaining equations (3.1)–(3.7), R_k^n simply scales. That is, for $\Delta r \to \Delta r/2$ and $\Delta t \to \Delta t/2$, then $R_k^n(\Delta r/2, \Delta t/2) = \frac{1}{2}R_k^n(\Delta r, \Delta t)$. Let us prove this. We take

$$\lambda = \Delta t/\Delta r \tag{4.1}$$

to be a constant, and from (2.2) and (3.8) we define a more general difference formulation of Q_L (which reduces to (3.8) for $l = \Delta r$); namely,

$$Q_L(\Delta r, C_0, C_1, l) = \left(C_0 \frac{l}{\Delta r}\right)^2 \rho(\Delta \bar{u})^2 - \left(C_1 \frac{l}{\Delta r}\right) \rho C_s \Delta \bar{u}, \tag{4.2}$$

from which it follows that

$$Q_L(\Delta r/N, C_0, C_1, l) = Q_L(\Delta r, NC_0, NC_1, l). \tag{4.3}$$

That is, holding l *fixed* (and equal to Δr in (4.2)) and letting $\Delta r \to \Delta r/N$ is simply equivalent to letting $C_0 \to NC_0$ and $C_1 \to NC_1$ in (3.8). To show the scaling of R_k^n in (3.1) to (3.8), we note that

$$R_k^{n+1}(\Delta r, \Delta t) = k\,\Delta r + \Delta t \sum_{i=0}^{n} u_k^{i+1/2} = \Delta r \left[k + \lambda \sum u_k^{i+1/2} \right] = \Delta r R_k^{n+1}(1, \lambda), \tag{4.4}$$

which completes the proof.

Thus, for example, if we let $\Delta r \to \Delta r/2$ (and since λ is constant, then $\Delta t \to \Delta t/2$), we find from (4.4) that

$$R_k^n(\Delta r/2, \Delta t/2) = (\Delta r/2)\, R_k^n(1, \lambda) = (1/2)\, R_k^n(\Delta r, \Delta t), \tag{4.5}$$

as noted above, and from (4.2),

$$Q_L(\Delta r/2, C_0, C_1, l) = Q_L(\Delta r, 2C_0, 2C_1, l), \tag{4.6}$$

which for $l = \Delta r$ is simply equal to $Q_L[(2C_0)^2, 2C_1]$ in the notation of (3.8). From (4.5) and (4.6) (i.e., letting $\Delta r \to \Delta r/2$), we can compute

$$\rho_{k+1/2}^n(\Delta r/2, \Delta t/2, C_0, C_1, l) = \rho_{k+1/2}^n(\Delta r, \Delta t, 2C_0, 2C_1, l), \tag{4.7}$$

and the refined mesh results can then be plotted by using (4.5) and (4.7). That is, we find the left side of (4.7) by simply letting $C_0^2 \to (2C_0)^2$ and $C_1 \to 2C_1$ in (3.8) and plot these results (which will be in terms of Δr and Δt) using (4.5).

This provides us with another interpretation of Fig. 2; calculating (using (3.8)) with $Q_L(4, \frac{2}{3})$ (i.e., $C_0^2 = 4$ and $C_1 = \frac{2}{3}$) is identical to using (4.2) with $l = 0.01$, $C_0 = 1$, and $C_1 = 0.33$ and to a mesh refinement of $\Delta r/2 = 0.005$. That is, from (4.2) $Q_L(0.005,\ 1,\ \frac{1}{3},\ 0.01) = \rho(0.01)^2\,|\Delta u/0.005|^2 - \frac{1}{3}\rho C_s(0.01)\,|\Delta u/0.005| = 4\rho\,|\Delta u|^2 - \frac{2}{3}\rho C_s\,|\Delta u|$, which is just $Q(4, \frac{2}{3})$ in our usual notation for (3.8). Also, if curve 2 of Fig. 2 is plotted letting $R_k^n \to (\frac{1}{2})R_k^n$ (i.e., a plot of $(\rho_k^n, (\frac{1}{2})R_k^n)$), it then represents a mesh refinement of curve 1 (holding $l = 0.01$ fixed). This is done in Fig. 4, and we

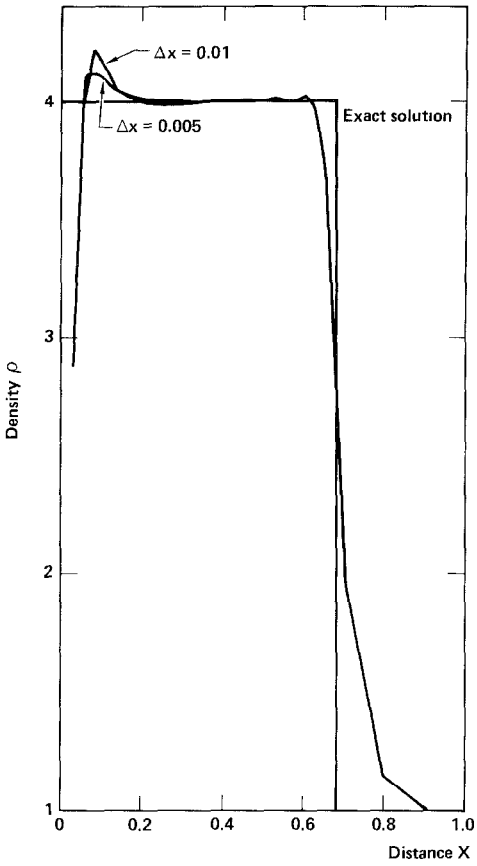

FIG. 4. For this calculation we compare $\Delta x = 0.01$ with $\Delta x = 0.005$ and evaluate $R_k^n(\Delta x/2, \Delta t/2)$ as $\frac{1}{2}R_k^n(\Delta x, \Delta t)$. That these two curves have the same wall heating error proves (as argued in Section 4.2) that the wall heating error is really an error in the **exact** solution of the hydrodynamic equations (2.1) with Q. That is, the curve labeled $\Delta x = 0.005$ is equivalent to a mesh refinement of 2 (where $\Delta x \to \Delta x/2$ and $\Delta t \to \Delta t/2$) of the curve labeled $\Delta x = 0.01$, and it is clear that the solutions are essentially converged. This also gives the correct interpretation of the results of Fig. 2.

see that the difference solution is essentially unchanged with respect to the wall heating error.[4]

We conclude, then, that wall heating is inevitable for our difference solution, since it already occurs in the exact solution of the differential equations (2.1) with Q given by (2.2). (The same conclusions hold for any Q formulation using similar arguments, or indeed for any shock-smearing method, as observed by Colella and

[4] The overshooting in density is also reduced for $\Delta r = 0.005$ (i.e., letting $\Delta r \to \Delta r/2$); indeed, this overshooting error would vanish as $\Delta r \to 0$. However, the wall heating error would remain. Thus, the wall heating error is indeed part of the solution of the differential equations with Q and depends on the size of the length, l—here, $l = 0.01$.

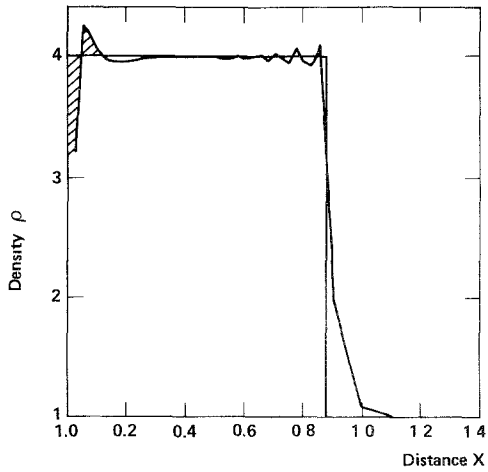

FIG. 5. $Q_L = \frac{2}{3}\rho(\Delta u)^2 - \frac{1}{5}\rho C_S \Delta u$. These small Q_L constants C_0 and C_1 reduce the wall heating error, but do not eliminate it.

Woodward [7]. Their more general result follows from total-energy considerations, which show that, in shock smearing, too much work is done when a shock starts up, or as here, when a shock is formed by bringing the gas to rest. Thus, wall heating is inherent in all such shock-smearing procedures.)

In real fluids, heat conduction is present, and excess wall heating cannot occur (since any hot spot would be quickly dissipated). This is the basis of Noh's (Q & H) method ((2.1) and (2.3)), which approximates nature more closely by using an artificial heat flux H (in conjunction with the usual artificial viscosity Q) to smear

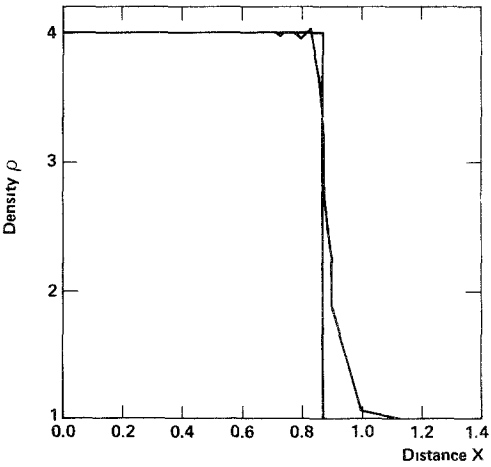

FIG. 6. $Q_L(\frac{2}{3}, \frac{1}{5}) = \frac{2}{3}\rho(\Delta u)^2 - \frac{1}{5}\rho C_S(\Delta u)$, and $H_L(0, \frac{3}{4}) = \frac{3}{4}\rho C_S \Delta\varepsilon$. This is the same Q used in Fig. 5, but now the artificial heat flux H is included in the energy equation, and the wall heating error has been eliminated. We also note that the shock solution is smoother using H (in conjunction with Q).

out shock discontinuities. In Fig. 5, one should compare $Q_L(C_0^2, C_1) = Q_L(\frac{2}{3}, \frac{1}{5})$ with Fig. 6, where $Q_L(\frac{2}{3}, \frac{1}{5})$, and the heat flux $H_L(0, \frac{3}{4}) = (\frac{3}{4})\rho C_s \Delta\varepsilon$ is used. As expected, the wall heating error is zero. We also note that the $(Q_L \& H_L)$ solution is considerably smoother. Indeed, this is one of the chief advantages of the (Q & H) method; namely, it permits the use of much smaller Q constants C_0^2 and C_1 (which, in general, reduces Q errors) and still maintains a smooth (or smoother) shock profile.

5. Shockless Q Heating Errors

This is the situation where a compression wave exists (and thus $u_r < 0$ and $Q \neq 0$), yet the exact solution is shockless. For this analysis, we consider the useful uniform collapse problem (see [5, p. 60]), in which a flow is everywhere undergoing a compression, but no shock develops. We consider a unit "sphere" $(0 \leqslant r \leqslant 1)$ (for planar, cylindrical, and spherical geometries; i.e., for $\delta = 1$, 2, or 3), and to simplify the analysis (of the energy errors due to Q) we take the pressure to be just a function of density: $P = P(\rho)$.

The initial values are $u(r, 0) = -r$, $\rho = \rho^0$, $\varepsilon = \varepsilon^0$, and $P^0 = P(\rho^0)$. The boundary conditions are $u(0, t) = 0$ and $u(1, t) = -1$. The exact solution is that the fluid simply coasts with its initial velocity ($u^0 = -r$) until all points uniformly collapse onto the origin $R = 0$, at time $t = 1$. It is easy to verify that the exact solution is given by

$$u(r, t) = -r, \qquad R = r(1 - t) \qquad \text{and} \qquad v = (1/\rho) = (1 - t)^\delta (1/\rho^0). \tag{5.1}$$

Thus, $\rho = \rho(t)$, $P = P(\rho) = P(t)$, and since $\varepsilon_t = -Pv_t = \delta/\rho^0 P(t)(1 - t)^{\delta - 1}$, then also $\varepsilon = \varepsilon(t)$, and no shocks are present. We now show that $Q = Q(t) \neq 0$, and thus Q will modify the exact solution. From (5.1), we let $\tau = (1 - t)$, from which $\rho = \rho^0 \tau^{-\delta}$, and we calculate Q_L, Q_E, and $Q_L(v)$,

$$Q_L = (C_0 l)^2 \rho (u_r)^2 = (C_0 l)^2 \rho^0 \tau^{-\delta}, \tag{5.2}$$

(which is not set to zero, since it passes the test $u_r = -1 < 0$). Also, $u_R = u_r / R_r = -\tau^{-1} < 0$, and thus $Q_E \neq 0$ and

$$Q_E = (C_0 l)^2 \rho (u_R)^2 = (C_0 l)^2 \rho^0 \tau^{-(\delta + 2)}. \tag{5.3}$$

Likewise,

$$Q_L(v) = (C_0 \rho^0 l)^2 \rho \left(\frac{r}{R}\right)^{2\delta - 2} (v_t)^2 = \delta^2 (C_0 l)^2 \rho^0 \tau^{-\delta}, \tag{5.4}$$

since $v_t = -(\delta/\rho^0)\tau^{(\delta - 1)} < 0$.

In particular, we note that

$$Q_L(v) = \delta^2 Q_L, \tag{5.5}$$

thus $Q_L \leqslant Q_L(v)$. Also,

$$Q_L = \tau^2 Q_E \leqslant Q_E \qquad (\text{as } \tau \leqslant 1); \tag{5.6}$$

Consequently, Q_L will produce the least error. This Q error occurs only in the energy equation, since $Q = Q(t)$, and thus, in the momentum equation $Q_r = 0$. To examine this Q error in energy, let $\Delta\varepsilon = \int(\varepsilon_t + Pv_t)\,dt = -\int Qv_t\,dt$. Then,

$$\Delta\varepsilon_L = -\int Q_L v_t\,dt = -\delta(C_0 l)^2 \log_e(\tau) > 0 \qquad (\text{as } \tau < 1), \tag{5.7}$$

$$\Delta\varepsilon_E = -\int Q_E v_t\,dt = \tfrac{1}{2}\delta(C_0 l)^2 \tau^{-2}, \tag{5.8}$$

$$\Delta\varepsilon_L(v) = -\int Q_L(v)\, v_t\,dt = -\delta^3(C_0 l)^2 \log_e(\tau) > 0. \tag{5.9}$$

Now, as in (5.5) and (5.6), we find

$$\Delta\varepsilon_L(v) = \delta^2\,\Delta\varepsilon_L \qquad \text{and} \qquad \Delta\varepsilon_L \leqslant \Delta\varepsilon_E. \tag{5.10}$$

and indeed Q_L produces the least **uniform collapse** Q error.[5]

Now, as $\tau \to 0$, the above errors $\Delta\varepsilon \to \infty$; and consequently, this shockless Q heating error can, under some circumstances, be serious indeed. From (5.10), we see that $\Delta\varepsilon_E > \Delta\varepsilon_L$, and this helps explain why the wall heating error for Q_E was larger than for Q_L, with the same C_0 and C_1 in Fig. 3. (This comparison is appropriate, since the first zone of problem 1 has precisely the same initial condition as for the problem of **uniform collapse**.) A more serious matter is the error $\Delta\varepsilon_L(v)$, which, for spherical geometries ($\delta = 3$), is nearly an order of magnitude greater than the error $\Delta\varepsilon_L$. In 1956, because of arguments similar to these, Noh [5, p. 58] suggested that Q_L of (2.2) be taken as the **standard** Q formulation for all geomerties $\delta = 1$, 2, or 3. We make the suggestion again (and for more reinforcement see Figs. 18 and 19), since $Q_L(v)$ still seems to be in common use.

6. Q Errors for a Nonuniform Mesh

The second type of Q error occurs when shocks are propagated over a mesh with unequal intervals. For our test problem 2, we again consider test problem 1, but now we introduce a nonuniform mesh with

$$\Delta x_{k+1} = R\,\Delta x_k, \tag{6.1}$$

where R is a constant: $R > 1$. We investigate the cases $R = 1.05$, $R = 1.15$, and $R = 1.25$. To show the errors for both decreasing and increasing mesh intervals, we let the mesh decrease for the first half of our test problem (i.e., let $R \to R^{-1}$ in (6.1)), and then we let the mesh increase (i.e., use (6.1)) for the second half (Fig. 7). In Fig. 8, $R = 1.05$, and the density is plotted for our **standard** $Q_L = 2\rho(\Delta u)^2$. The total error is shaded, and again we see the familiar wall heating error in the first several zones. The new error: $\Delta\rho_L^+ = \rho_L^+ - \rho_{\text{exact}}^+ = \rho^+ - 4$ is too large (i.e., $\Delta\rho_L^+ \geqslant 0$)

[5] Several Q_L formulations have been proposed [6, 8] for which the shockless Q energy error vanishes (i.e., $\Delta\varepsilon = 0$), but, unfortunately, they do not otherwise represent a general fix to the remaining Q errors in shock tracking that we consider here.

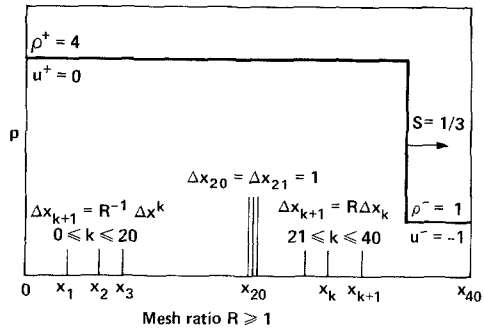

FIG. 7. The unequal-zoned, infinite-shock test problem. The initial and boundary conditions are the same as in test problem 1, but here the initial zoning varies geometrically with $\Delta x_{k+1} = R\Delta x_k$ (for constant $R > 1$). The mesh interval Δx_k decreases ($\Delta x_{k+1} = R^{-1}\Delta x_k$) for the first half of the mesh ($0 \leqslant k \leqslant 20$), then Δx_k increases ($\Delta x_{k+1} = R\Delta x_k$) for the second half. The problems are normalized (for any ratio R) by taking $\Delta x_{20} = \Delta x_{21} = 1.0$. The **exact** solution, of course, is the same as in problem 1 and is shown for $\gamma = \frac{5}{3}$. That is, $\rho^+ = 4$, and the shock speed $S = \frac{1}{3}$.

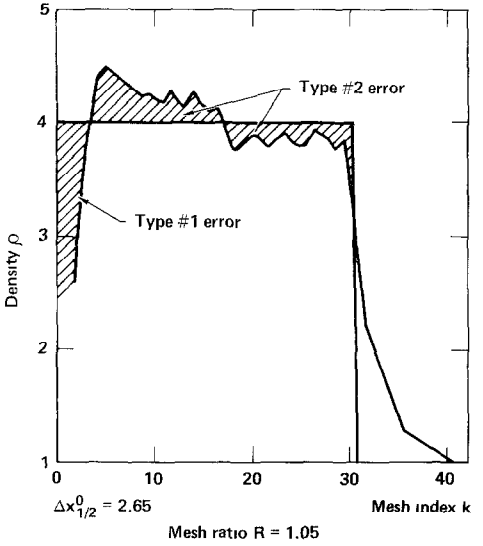

FIG. 8. Here $R = 1.05$, and this is the **standard calculation** using the **benchmark** $Q_L(2, 0) = 2\rho(\Delta u)^2$. This type 2 error, $\Delta\rho^+ = \rho^+ - 4$, is positive for the first half of the mesh ($0 \leqslant k \leqslant 20$), where the mesh interval decreases (i.e., $R^{-1} < 1$) and is negative (i.e., $\Delta\rho^+ < 0$) for the second half ($21 \leqslant k \leqslant 40$), where the mesh interval increases ($R > 1$). The type 1 wall heating error is still present in the first few zones next the rigid wall on the left; we note that here, $\Delta x_{1/2} = 2.65$ (compared with $\Delta x_{1/2} = 1.0$ in test problem 1), and hence, this wall heating error is more serious than it may appear.

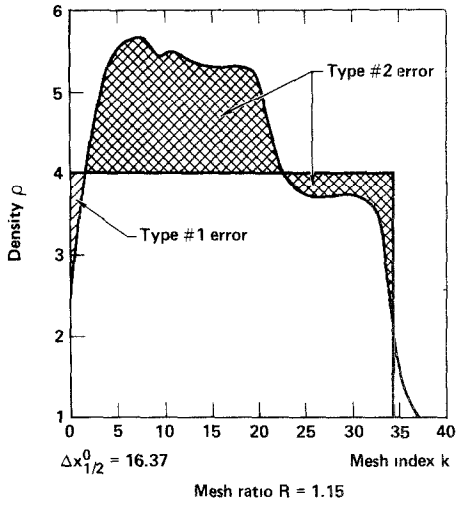

FIG. 9. Standard calculation using $Q_L(2,0) = 2\rho(\Delta u)^2$, with $R = 1.25$. Here we note that $\Delta x_{1/2} = 16.37$; thus both the type 1 and type 2 errors are very large.

for the first half of the problem, where the mesh decreases, and too small ($\Delta\rho_L^+ < 0$) for the second half, where the mesh interval increases.

In Fig. 9, $R = 1.15$, and in Fig. 10, $R = 1.25$. The wall heating (type 1) error is almost the same in each problem (in the sense that it is still just over the first several zones), but here the first few zones are larger, with larger values of R, and thus the error becomes more serious as R increases. The new (type 2) nonuniform mesh error also grows with R and becomes very serious ($\simeq 100\%$) for $R = 1.15$.

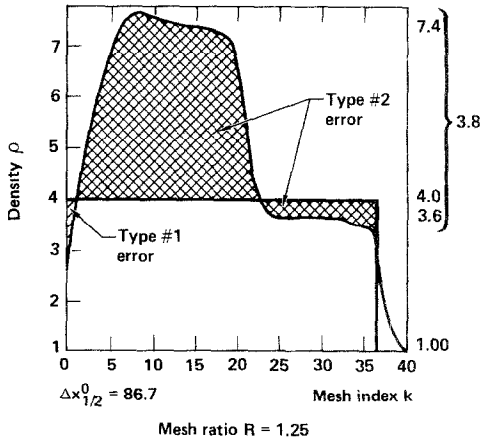

FIG. 10. **Standard** $Q_L(2,0) = 2\rho(\Delta u)^2$. $R = 1.25$, and the type 2 error is nearly 100%. Here $\Delta x_{1/2} = 86.7$, and the type 1 error is also enormous.

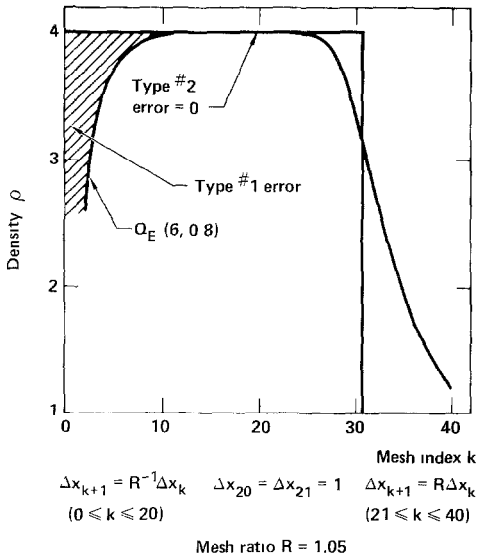

FIG. 11. Here $R = 1.05$, and the Eulerian (fixed-length) Q_E is used, which spreads shocks over a fixed physical distance: $Q_E(6, \frac{4}{5}) = 6\rho(\Delta u/\Delta x)^2 - \frac{4}{5}\rho C_S(\Delta u/\Delta x)$, and the type 2 error vanishes (i.e., $\Delta\rho_E^+ = \rho_E^+ - 4 = 0$). However, the wall heating (type 1) error is now very large using Q_E, due to the large constants $C_0 l$ (and $C_1 l$) that are required to spread the shock over approximately three of the largest mesh intervals. (That is, for $R = 1.05$, $l = \Delta x_{\max} = \Delta x_{1/2} = 2.65$; and we take $C_0 \simeq 0.9$ and $C_1 \simeq 0.3$. As a comparison, see Fig. 3, where for Q_E, with $\Delta x = 1$, we used $C_0 = 1$ and $C_1 = 0.33$.)

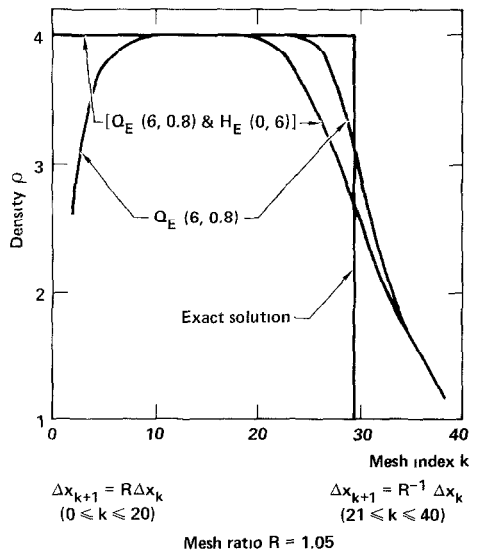

FIG. 12. Here we compare the Eulerian (fixed-length) Q with the (Q_E & H_E) method and the exact solution. Here, $Q_E(6, \frac{4}{5}) = 6\rho(\Delta u/\Delta x)^2 - \frac{4}{5}\rho C_S(\Delta u/\Delta x)$ (see Fig. 11), and we use $Q_E(6, \frac{4}{5})$ and $H_E(0, 6)$, where $H_E(0, 0.6) = 6\rho C_S \Delta\varepsilon$. Now, both the type 1 wall heating error and the nonuniform mesh type 2 error are eliminated. However, there is too much shock spreading using Q_E for this to be a practical solution to minimizing these errors.

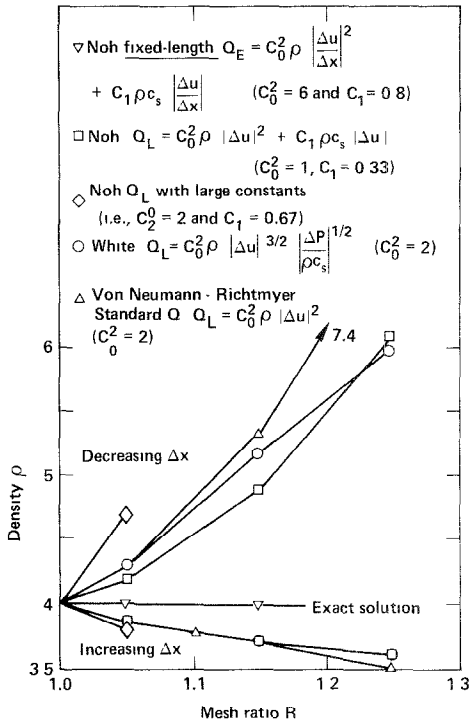

FIG. 13. Nonuniform mesh $\Delta x_{k+1} = R\Delta x_k$ of Fig. 7, comparing various Q formulations [1, 5, 6] and their type 2 error, $\Delta\rho^+ = \rho^+ - 4$. Here, only the Eulerian formulation Q_E gives $\Delta\rho_E^+ \equiv 0$ (i.e., using a fixed-length Q_E, the type 2 error vanishes). We note that all Lagrange formulations Q_L (i.e., where $l = \Delta x$), produce $\Delta\rho_L^+ \neq 0$ (i.e., a type 2 nonuniform mesh Q error occurs). We see that this error grows with the magnitude of C_0^2 and also with $(R-1)$; thus, $\Delta\rho_L^+ \sim C_0^2(R-1)$.

This is unfortunate, as it is not uncommon to use $R = 2$ in practice, and thus $R = 1.25$ might well be considered a modest zoning change.

The good news is shown in Fig. 11, where $R = 1.05$ and the Eulerian, fixed length Q_E of (2.4) and (3.9) eliminates the nonuniform mesh error completely. The bad news is that very large Q_E constants are necessary (i.e., for $\Delta x_{max} = \Delta x_{1/2} = 2.65$, then $(C_0 l)^2 = (C_0 \Delta x_{max})^2 = 6$ (for $C_0 \simeq 0.9$) and $C_1 \Delta x_{max} = 4/5$ (for $C_0 \simeq 0.3$]. This is seen to spread the shock over a large number of the smaller zones, and, in this regard, the use of Q_E is not satisfactory. Also, the use of Q_E generates a very large type 1 (wall heating error) at the wall [see the discussion of (5.10)].

In Fig. 12, the $(Q_E \& H_E)$ method is tested for $R = 1.05$, which results in both the type 1 and the type 2 errors going to zero. Thus, in principal, we have a complete remedy by using the fixed-length (E) formulation for both Q and H. However, as mentioned above, this is not generally a satisfactory solution because of the exessive spreading of shocks by the use of Q_E.

In Fig. 13, the results of several Lagrangian Q_L's (i.e., where $l = \Delta x$) all give essentially the same error (where the larger errors correspond to the use of larger constants C_0^2 and C_1), and we see that only Q_E eliminates the nonuniform mesh error completely. In particular, we note that the nonuniform mesh error goes roughly as

$$\Delta\rho_L^+ \simeq C_0^2(R-1). \tag{6.2}$$

That is, this error increases with the Q_L constant C_0 (see also Figs. 15 and 16 in Section 7) and with the fractional change in mesh width $(R-1)$. Also, the term $(R-1)$ accounts for the change in sign of the error for $R>1$ or $R<1$. We also note that White's [6] Lagrangian Q_L (which was designed, in part, to eliminate the uniform collapse error of Section 5) here fares no better (or worse) than the other Lagrangian Q_L formulations. This leads us to conclude that the uniform collapse error is independent of the type 2 (nonuniform mesh) error.

7. Theoretical Discussion

In the standard difference formulations of Q_L, the length l in (2.2) is taken to be $l_{k+1/2} = \Delta x_{k+1/2}$, which gives $(lu_x)_{k+1/2} = (\Delta u)_{k+1/2}$ in (3.7). Now, when an unequal mesh interval is used, setting l equal to $\Delta x_{k+1/2}$ (which is no longer a constant) implies that l is a function of x. That is, in the differential formulation (2.2) of Q_L, $l = l(x)$. We wish to determine $l(x)$, where $\Delta x_{k+1/2}$ is given by (6.1), or what is equivalent,

$$\Delta x_{k+1/2} = R^k \Delta x_{1/2}. \tag{7.1}$$

After a certain amount of algebra, we find that $l(x)$ is given by

$$l(x) = 2[(R-1)x + \Delta x_{1/2}]/(R+1). \tag{7.2}$$

Let us verify that, indeed, $l_{k+1/2} = \Delta x_{k+1/2}$. Note that (7.1) implies

$$x_k = \left(\frac{1-R^k}{1-R}\right)\Delta x_{1/2}, \tag{7.3}$$

and we substitute this into (7.2). Collecting terms and using (7.1), we have

$$\begin{aligned} l_{k+1/2} &= l\left(\frac{x_{k+1}+x_k}{2}\right) \\ &= \left\{2(R-1)\left[\frac{1-R^{k+1}+1-R^k}{2(1-R)}\right]\Delta x_{1/2} + \Delta x_{1/2}\right\} \div (R+1) \\ &= R^k \Delta x_{1/2} = \Delta x_{k+1/2}, \end{aligned}$$

as required. Thus, the differential formulation of Q_L is given by

$$Q_L = C_0^2 \rho l(x)^2 (u_x)^2 - C_1 \rho l(x)(u_x), \qquad \text{if} \quad u_x \leqslant 0, \tag{7.4}$$

where $l(x)$ is given by (7.2).

One consequence of using (7.4) instead of (2.2) in the differential equations (2.1) is that steady traveling shocks are no longer solutions. To see this, we note that the shock width (which is proportional to l) will now be proportional to $l(x)$ and means that the shock shape changes with space and thus with time. This might still be an acceptable Q representation of shocks, if only the proper shock-jump conditions held, but our numerical experiments show, unfortunately, that this is not the case.

Let us examine more closely the error introduced by $l = l(x)$. We suppose that Q is given by (7.4), and for simplicity, we take Q to be linear in u_x (i.e., $C_0^2 = 0$ and $\rho C_s = \rho^0 C_s^0 =$ a constant). Then, Q is given by

$$Q = -C_1 \rho^0 C_s^0 l(x) u_x. \tag{7.5}$$

We want to show that (7.5) (with $R \neq 1$ in (7.2)) introduces a fundamental error in the differential equations.

We examine the momentum equation, $u_t = -(1/\rho^0) P_x - (1/\rho^0) Q_x$, and from (7.5) we write

$$u_t = -(1/\rho^0) P_x + C_1 C_s^0 l u_{xx} + [(C_1 C_s^0) u_x] \, l_x. \tag{7.6}$$

From (7.2), we have $l_x = 2(R-1)/(R+1)$, and thus (7.6) can be written (letting $\bar{C}_s = 2C_s^0 \div (R+1)$) as

$$u_t - C_1 (R-1) \, \bar{C}_s u_x = \frac{-1}{\rho^0} P_x + C_1 C_s^0 l u_{xx}. \tag{7.7}$$

We interpret the left-hand side of (7.7) as arising from a fictitious frame-of-reference velocity $\dot{X}$ given by

$$\dot{X} = u + C_1 (R-1) \bar{C}_s. \tag{7.8}$$

We deduce this by the following argument. In general, time derivatives are given by $\dot{f} = f_t + (u - \dot{X}) f_x$; where $X = X(x, t) = x + \int \dot{X} \, dt$ is the Eulerian coordinate of a general time-dependent frame of reference. For instance, if $\dot{X} = u$, then $\dot{f} = f_t$, and $X(x, t) = x + \int u \, dt$ is just the Lagrange reference frame. If $\dot{X} = 0$, then $\dot{f} = f_t + u f_x$, and $X(x, t) \equiv x$, which is the Eulerian frame of reference. Thus, from (7.7), $u - \dot{X} = -C_1 (R-1) C_s^-$, and it follows that $\dot{X}$ is given by (7.8). This is just the behavior we observed in our numerical experiments (see (6.2)). That is, from (7.1), $R < 1$ gives a decreasing interval, and (7.8) implies that $\dot{X} < u$, or the frame-of-reference velocity is too slow, which (since the mass of a zone is constant) gives ρ^+ too large. Likewise, for $R > 1$, then $\dot{X} > u$, and ρ^+ is too low (see Figs. 8, 9, and 10).

In addition to this error in the momentum equation, a more serious error enters

the energy equation. To see this, let us revisit the uniform collapse problem of Section 5 and again take Q to be given by (7.5). The exact solution in plane geometry ($\delta = 1$) for the uniform collapse problem, where the initial conditions are $u(x, 0) = -x$ and $P = P(\rho)$, is again found by assuming $\rho = \rho(t)$, and thus $P = P(t)$. Doing this, we check by direct substitution into (7.7), that the solution is given by

$$u(x, t) = -x - C_1(R-1)\bar{C}_s t. \tag{7.9}$$

Then, from $X = x + \int u\, dt$,

$$X = x(1-t) - (1/2)\, C_1(R-1)\, \bar{C}_s t^2, \tag{7.10}$$

and from (2.1), $v = X_m = (1/\rho^0)X_x = (1/\rho^0)(1-t)$; or, since $v = 1/\rho$,

$$\rho = \rho^0/(1-t). \tag{7.11}$$

Thus, as required, $\rho = \rho(t)$ and $P = P(t)$. Indeed, (7.9) is the **exact** solution, with Q given by (7.5). We can now compute the Q energy error, $\Delta\varepsilon$, where

$$\Delta\varepsilon = \int (\varepsilon_t + Pv_t)\, dt = -\int Qv_t\, dt = \int C_1 \rho^0 C_s^0 l(x)\, u_x v_t\, dt = C_1 C_s^0 l(x) t.$$

Now, $l(x)$ is given by (7.2), and thus

$$\Delta\varepsilon = +2C_1 C_s^0 \{[R-1)x + \Delta x_{1/2}]/(R+1)\} t. \tag{7.12}$$

Equation (7.9) shows that the **momentum error** goes as $C_1(R-1)t$, while (7.12) shows that the **energy error** is more serious, as it depends on x as well as t, and goes as $C_1(R-1)xt$.

There is still the question of how closely the difference solution agrees with our analytical results. For the **uniform collapse** problem, at least, the agreement is **exact**. We mean by this that the solution to the difference equations (3.1)–(3.6) over the **nonuniform mesh:** $x_k = [(1-R^k) \div (1-R)]\, \Delta x_{1/2}$, with Q_L given by (7.5) and $l(x)$ given by (7.2) (which, for the difference equations, is the same as using $Q_L = -C_1 \rho^0 C_s^0\, \Delta u$), is precisely given by (7.9) to (7.11). To show this, we let $u_k^{n+1/2} = u[x_k, (n+\tfrac{1}{2})\, \Delta t]$, $\rho_{k+1/2}^{n+1} = \rho[(x_k + x_{k+1})/2, (n+1)\, \Delta t]$, etc. Then, from (7.9) and (7.3),

$$\begin{aligned} u_k^{n+1/2} &= -x_k - C_1(R-1)\, \bar{C}_s(n+\tfrac{1}{2})\, \Delta t \\ &= \frac{1-R^k}{1-R}\, \Delta x_{1/2} - C_1(R-1)\, \bar{C}_s(n+\tfrac{1}{2})\, \Delta t, \end{aligned} \tag{7.13}$$

and similar substitutions in (7.11) give $\rho_{k+1/2}^{n+1}$, etc. It is easy to verify that (7.13) etc. exactly satisfies (3.1) to (3.6).

That the difference solution (7.13) is precisely the **exact** solution (7.9) is no doubt a function of the simplicity of this **uniform collapse** test problem, but it does confirm

our analysis that the source of error arises from letting $l = \Delta x$ in the Lagrangian Q_L difference formulation. Also, it is easy to verify that if Q_E of (3.9) is used in the **uniform collapse** test problem, then (as in our experiments) the difference solution is also the **exact** solution, without Q, and is thus independent of the mesh interval. Consequently, our theory is in exact agreement with our numerical results—at least for this simple **uniform collapse** problem.

For the general case of a nonuniform mesh (i.e., test problem 2), we argue by numerical experiment that the source of difficulty indeed lies in allowing $l = \Delta x$ in the difference approximation of the Lagrangian Q_L formulation, which, in turn, implies that $l = l(x)$ in the **differential equation** formulation of Q_L. That is, we want to show that the numerically observed nonuniform mesh error is simply due to the error in the solution of the **differential equations** when Q_L is given by (7.4). We do this by using the Q_L of (7.4) and $l = l(x)$ of (7.2) in Eqs. (2.1) and solving test problem 1 (which is just test problem 2 with equal mesh intervals). This leads to the difference equations (3.1)–(3.6) with $(Q_L)_{k+1/2}$ of (7.4) given by

$$(Q_L)_{k+1/2} = C_0^2 \rho_{k+1/2} \left[l(x) \frac{\Delta u}{\Delta x} \right]^2_{k+1/2} - C_1 \rho_{k+1/2} (C_s)_{k+1/2} \left[l(x) \frac{\Delta u}{\Delta x} \right]_{k+1/2}, \tag{7.14}$$

where now (for **equal mesh intervals:** $\Delta x_{k+1/2} \equiv \Delta x_{1/2}$) $[l(x)\, \Delta u/\Delta x]$ is given by

$$\left[l(x) \frac{\Delta u}{\Delta x} \right]_{k+1/2} = 2\{[(R-1)(k+\tfrac{1}{2})+1]/(R+1)\}[\Delta u]_{k+1/2}. \tag{7.15}$$

We want to show, then, that both **equal** and **unequal** zoning lead to essentially the same numerical solution. This numerical solution, in turn (we assume), converges to the **exact** solution of the **differential equations** (2.1) with Q given by (7.4), and $l(x)$ given by (7.2). In particular, in Fig. 14, we use equal mesh intervals (i.e., $\Delta x_{k+1/2} \equiv \Delta x_{1/2}$) and take $R = 1.05$ in (7.15).

This choice of R corresponds to an increasing mesh interval; and, just as in the second half of test problem 2 (with $R = 1.05$, Fig. 8), the density is seen to be too low. More than that, the density in Fig. 14 is too low by exactly the same amount as in Fig. 8, which shows that this Q_L error is independent of the mesh interval used, and we conclude that we essentially have convergence to the exact solution.[6]

This establishes that it is the Lagrange formulation Q_L, where l is taken to be mesh interval Δx, that causes this Q error. Thus all Q_L formulations will presumably be equally in error by a similar argument, while only the fixed-length Q_E results are correct (Fig. 13).

[6] In Fig. 14, the results are smoother than in Fig. 8 due to the presence of a linear term in Q_L. In particular, in Fig. 14, we used $Q_L(C_0^2, C_1) = Q_L(1, \frac{1}{2})$ versus $Q_L(2, 0) = 2\rho(\Delta u)^2$ in Fig. 8. Of course, the wall heating Q error in Fig. 14 remains, since it is a Q error of type 1 and occurs for all Q's, as discussed in Section 4.2.

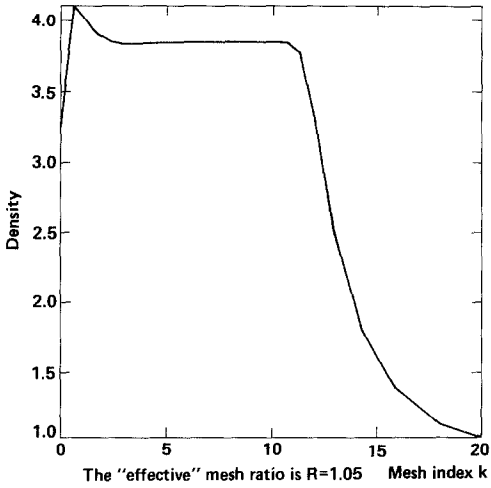

FIG. 14. Here we prove numerically that the nonuniform mesh error is due to the Lagrangian formulation of Q in which the standard usage is to take the length l equal to Δx (i.e., $l_{k+1/2} = \Delta x_{k+1/2}$). This implies (for an unequal mesh) that $l = l(x)$. In Section 7, we argue that an unequal mesh, given by $\Delta x_{k+1/2} = R\ \Delta x_{k-1/2}$, is equivalent to using (in the **differential equations**) $Q_L = C_0^2 \rho [l(x)]^2 (u_x)^2 - C_1 \rho l(x) u_x$ (i.e., (7.4)), where $l(x)$, is given by (7.2): $l(x) = 2[(R-1)x + \Delta x_{1/2}] \div (R+1)$. For this choice of Q_L and $l(x)$, we seek the **exact** solution of the **differential equations** and want to show that this solution contains what we have called the type 2 nonuniform mesh error. To do this, we difference the above Q_L and $l(x)$, assuming a constant $\Delta x_{k+1/2} = \Delta x_{1/2}$ for test problem 1. This is the same, then, as using $(Q_L)_{k+1/2} = C_0^2 \rho_{k+1/2} l_{k+1/2}^2 (\Delta u/\Delta x)_{k+1/2} - C_1 \rho_{k+1/2} (C_S)_{k+1/2} l_{k+1/2} (\Delta u/\Delta x)_{k+1/2}$, where (for equal Δx) we have $l_{k+1/2} = 2[(R-1)(k+1/2)+1] \div (R+1)$. For $R = 1.05$, this is seen to be identical to the calculation in Fig. 8—where we compare just the second half of the mesh ($21 \leqslant k \leqslant 40$) (i.e., where the mesh interval Δx increases). In this comparison, we see that the solutions are essentially the same (when we exclude the wall heating type 1 error above). (The solution shown is also smoother than in Fig. 8 due to the use here of a linear term in Q_L. Here, $Q_L(C_0^2, C_1) = Q_L(1, \frac{1}{2}) = \rho l^2(x)(\Delta u/\Delta x)^2 - \frac{1}{2}\rho l(x)\ C(\Delta u/\Delta x)$ vs the otherwise equivalent (but noisier) $Q_L = 2\rho(\Delta u)^2$ in Fig. 8.) The point here is that if the unequal mesh ($\Delta x_{k+1/2} = R\Delta x_{k-1/2}$) is used with the Q_L above (i.e., (7.4)) and $l(x)$ of (7.2), then Q_L reduces to the **standard** $Q_L = C_0^2 \rho (\Delta u)^2 - C_0 \rho C(\Delta u)$. Thus both the above calculation and the second half of the calculations in Fig. 8 are simply different approximations to the identical difference equations, but with equal mesh intervals (above) and unequal intervals in Fig. 8. Since these solutions agree, it is clear that the numerical solution is not sensitive to equal or unequal zoning, and we conclude that we essentially have convergence, and indeed the **unequal mesh error** is already an error in the **exact** solution of the **differential equations**. This completes the numerical proof.

A more practical solution to the nonuniform mesh error is to use the (Q_L & H_L) method. Using an artificial heat flux H_L not only eliminates the wall heating error, but also allows for smoother shocks, and thus smaller Q constants C_0^2 and C_1. This is shown by comparing Figs. 15 and 16. Figure 15 compares $R = 1.05$ and $Q_L = 2\rho(\Delta u)^2$ with the (Q_L & H_L) method—in both cases, $Q_L = 2\rho(\Delta u)^2$. In Fig. 16, we make the same comparison, but with $Q_L = \rho(\Delta u)^2$ (i.e., $C_0^2 = 1$), and we see that the (Q_L & H_L) method produces a corresponding reduction in the **nonuniform** zoning error to around 3%. In both Figs. 15 and 16, we see that the (Q_L & H_L)

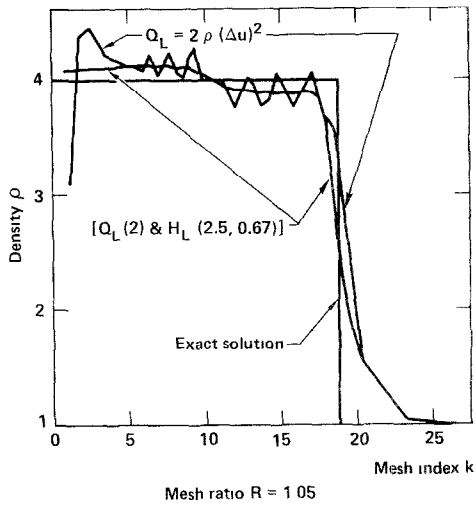

FIG. 15. $R = 1.05$, and we compare the Q_L and $(Q_L \& H_L)$ methods: $Q_L(2, 0) = 2\rho(\Delta u)^2$; and $Q_L(2, 0) = 2\rho(\Delta u)^2$ and $H_L(2.5, \frac{2}{3}) = 2.5\rho|\Delta u|\ \Delta\varepsilon + \frac{2}{3}\rho C_S\ \Delta\varepsilon$. As expected, the wall heating (type 1) error is eliminated when the heat flux term H_L is included.

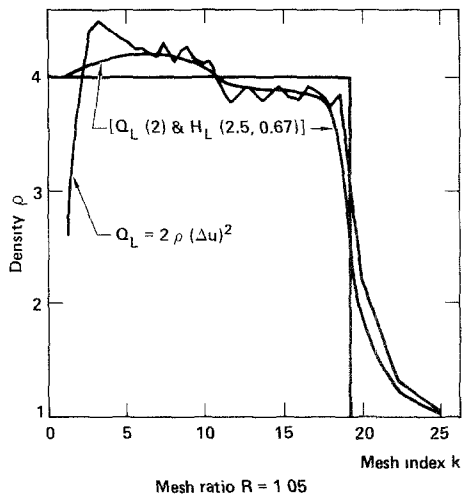

FIG. 16. $R = 1.05$, and we again compare Q_L (but here using a reduced coefficient $C_0^2 = 1$) with the $(Q_L \& H_L)$ method: $Q_L(1, 0) = \rho(\Delta u)^2$. The solution is noisy, but both types 1 and 2 errors are reduced by using this smaller value of C_0^2. $Q_L(1, 0) = \rho(\Delta u)^2$ & $H_L(0, \frac{2}{3}\rho C_S \Delta\varepsilon$. We see that using both Q_L and H_L eliminates the wall heating type 1 error altogether and (with small Q coefficients) reduces the type 2 non-uniform mesh error to $\simeq 3\%$. The $(Q_L \& H_L)$ method is much smoother than Q_L alone and may be a practical compromise for mesh-interval changes that are not too large.

method has eliminated the **wall heating** type 1 error. For modest values of R, then, the $(Q_L \& H_L)$ method may give sufficient accuracy; otherwise, the $(Q_E \& H_E)$ method is needed, and both the wall heating error and the nonuniform mesh error will be eliminated.

8. Q Errors in Spherical ($\delta = 3$) Geometry

The third type of Q error is related to strong shock propagation in spherical (or cylindrical) geometries. This error is considerably more serious (up to 1000% error in excess shock heating near the origin) and is also more complicated than the previous Q errors. This type 3 error depends on the Q formulation (i.e., Q_L of (2.2) vs $Q_L(v)$ of (2.6)), and also seems to depend on whether Q is treated as a scalar or a tensor viscosity in the formulation of the hydrodynamic equations. In particular, a tensor formulation due to Schulz [8] and one due to Whalen [9] produce less Q heating behind shocks and give sharper shocks than our **standard** Q_L formulation. Those sharper shocks and less central heating are instrumental in reducing this third type of Q error, and both of these tensor formulations are considered more appropriate in spherical geometry than the usual equations (2.1).

Test problem 3 is just the spherical ($\delta = 3$) generalization of test problem 1. Here the post-shock solution is, again, a set of constant-value step functions (u^+, ρ^+, ε^+, and P^+) (see Fig. 17d of Noh's generic, constant-velocity shocks). The initial conditions for the unit sphere ($0 \leqslant r \leqslant 1$) are $u(r, 0) = u^0 = -1$, $\rho(r, 0) = \rho^0 = 1$, $\varepsilon(r, 0) = \varepsilon^0 = 0$, and $P^0 = (\gamma - 1)\rho^0\varepsilon^0 = 0$, and the boundary conditions are $R(0, t) \equiv 0$ and $u(1, t) \equiv -1$. The **exact** solution (for $\gamma = \frac{5}{3}$) is given in Fig. 17d, where $u^+ = 0$, $\rho^+ = 64$, $\varepsilon^+ = \frac{1}{2}$, and $P^+ = (\frac{2}{3})\rho^+\varepsilon^+ = \frac{64}{3}$. The shock speed is $\dot{R}_s(t) = S \equiv \frac{1}{3}$. The preshock values are $u^- = u^0 = -1$, $\varepsilon^- = \varepsilon^0 = 0$, $P^- = P^0 = 0$, and the density in front of the shock is given by $\rho = \rho^0(1 + t/R)^2$. The shock position, $R_s = t/3$, gives the preshock density $\rho^- = (1 + t/R_s)^2 = (1 + 3)^2 = 16$, which we see is independent of t, and thus leads to the constant postshock values given above.

Our **standard** test problem has 100 mesh intervals ($\Delta r = 0.01$ and $K = 100$), and the results are compared at time $t = 0.6$. Since the shock speed is $S = \frac{1}{3}$, 80% of the mesh, or 80 mesh points, have been traversed by the shock, and one would expect accurate results.

Unfortunately, this is not the case. In Fig. 18, the **standard** $Q_L(2) = 2\rho(\Delta u)^2$ is compared with the **original** $Q_L(v) = 2(\Delta r)^2\rho(r/R)^4(\Delta v/\Delta t)^2 = 2\rho(\Delta u + 2u\,\Delta R/R)^2$ (see (3.12)), and both are compared with the **exact** solution $\rho^+ = 64$. The numerical results are strikingly poor and, in fact, hardly bear any resemblance to the **exact** solution. The error for the **standard** Q is seen to be on the order of 600% near the origin and 20% behind the shock, while the error for the original von Neumann–Richtmyer Lagrangian Q is roughly 1000% in the central region and nearly 40% behind the shock.

Clearly, this third type of Q error depends on the Q formulation. There are several reasons for this. One is related to the **shockless** Q **heating** error of Section 5,

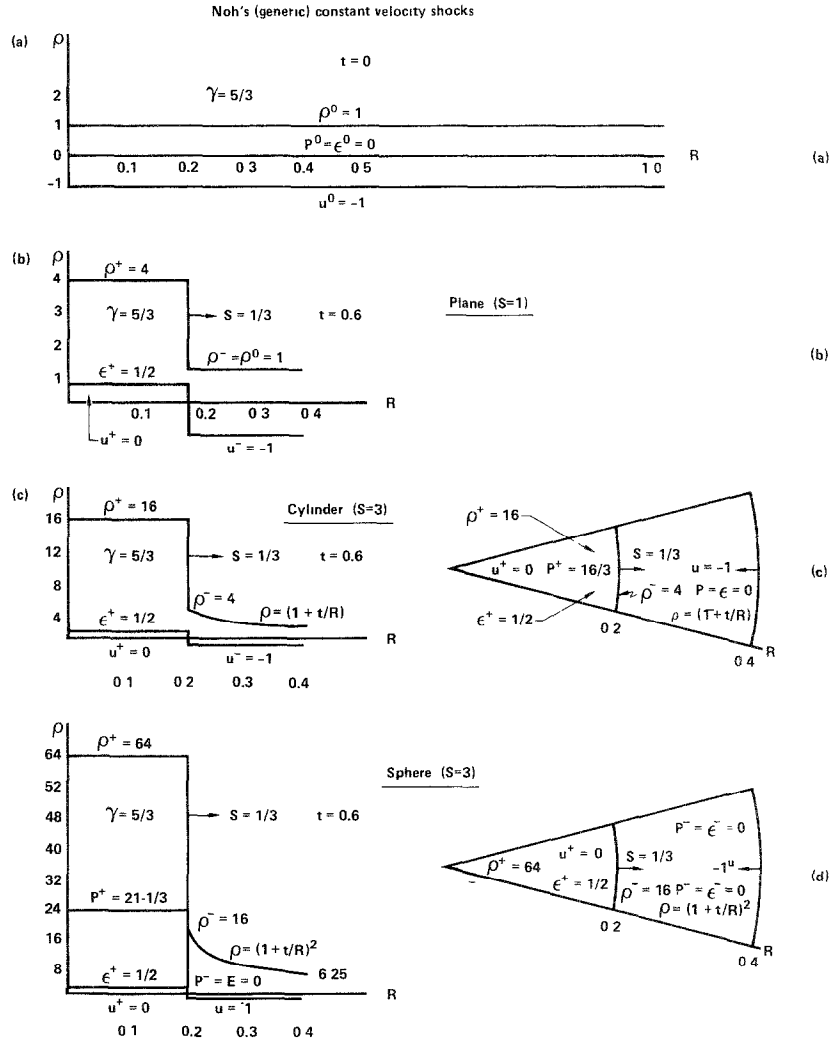

FIG. 17. The **exact** solution at $t = 0.6$ to Noh's generic, constant-velocity shock problems [2]: (a) initial conditions; (b) plane geometry ($\delta = 1$) with a shock generated at a rigid wall; (c) a shock generated at the axis of symmetry of a cylinder ($\delta = 2$); and (d) a shock generated at the center of a sphere ($\delta = 3$). All solutions have **constant post-shock states** and the same **constant shock speed** ($S = \frac{1}{3}$). The **essential difference** is the pre-shock density: $\rho^- = 1$ for $\delta = 1$, $\rho^- = 4$ for $\delta = 2$, and $\rho^- = 16$ for $\delta = 3$; and $\rho = \rho^0(1 + t/R)^{\delta - 1}$ in front of the shock.

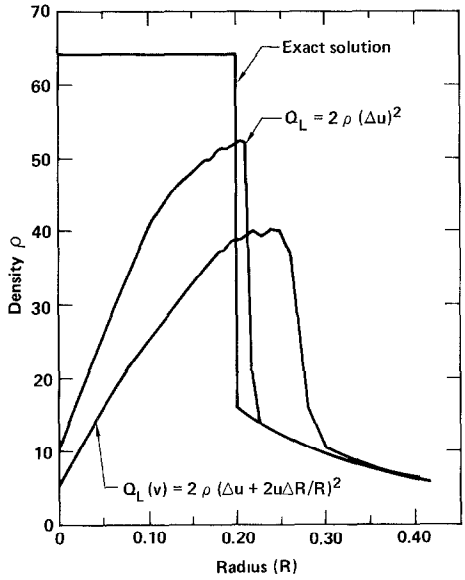

FIG. 18. This is the **benchmark** test problem, where $\Delta r = 0.01$ (i.e., $K = 100$) and time $t = 0.6$. Here we compare the **standard** $Q_L = 2\rho(\Delta u)^2$ with the original von Neumann–Richtmyer $Q_L(v)$ formulation, (2.6): $Q_L(v) = 2(\Delta r)^2\ \rho(r/R)^4(\Delta v/\Delta t)^2 = 2\cdot 10^{-4}\ \rho(r/R)^4\ (\Delta v/\Delta t)^2 = 2\rho[\Delta u + 2u\Delta R/R]^2$ (see (3.12)). Here Q_L is superior to $Q_L(v)$, but both Q's produce serious errors. The correct solution is $\rho^+ = 64$.

since the first zone of test problem 3 is just a special case of our **uniform collapse** test problem, and we found in (5.9) that the Q_L energy errors went as $\Delta\varepsilon_L(v) = \delta^2\,\Delta\varepsilon_L$. Thus, for $\delta = 3$, the error using $Q_L(v)$ is nine times as large as using Q_L.

An even more disquieting error arises from using the $Q_L(v)$ formulation of Q, which preheats the gas **ahead** of the shock. This occurs because, in the preshock region, $v = 1/\rho = (1 + t/R)^{-2}$, and thus, $v_t = -(2/R)(1 + t/R)^{-3} < 0$, from which it follows that $Q_L(v) \neq 0$. This preheating is, of course, not physical, but is another instance of a **shockless** Q **heating** error. Note, however, that our **standard** Q_L vanishes ahead of this shock. This error and the large **shockless** Q **heating** error near the origin combine to produce errors for $Q_L(v)$ considerably worse than those for Q_L, as shown in Fig. 18. Indeed, it is surprising that the solution is as good as it is.

Just how slowly the $Q_L(v)$ solution converges is shown in Fig. 19, where the results are plotted for various mesh intervals ($K = 50$ ($\Delta r = 0.02$) up to $K = 800$ ($\Delta r = 0.00125$)). Even at $K = 800$, the numerical solution still has a disquieting error. These results show that $Q_L(v)$ of (2.6) is a **poor formulation** and is essentially the reason that our definition of Q_L given by (2.2) is taken to be the **standard** Q (for $\delta = 1$, 2, and 3). We stress this point, since $Q_L(v)$ still seems to be in common use.

Now, of course, there are still serious errors in the use of the **standard** $Q_L = 2\rho(\Delta u)^2$. This difficulty is analyzed in Fig. 20. The problem is seen to be

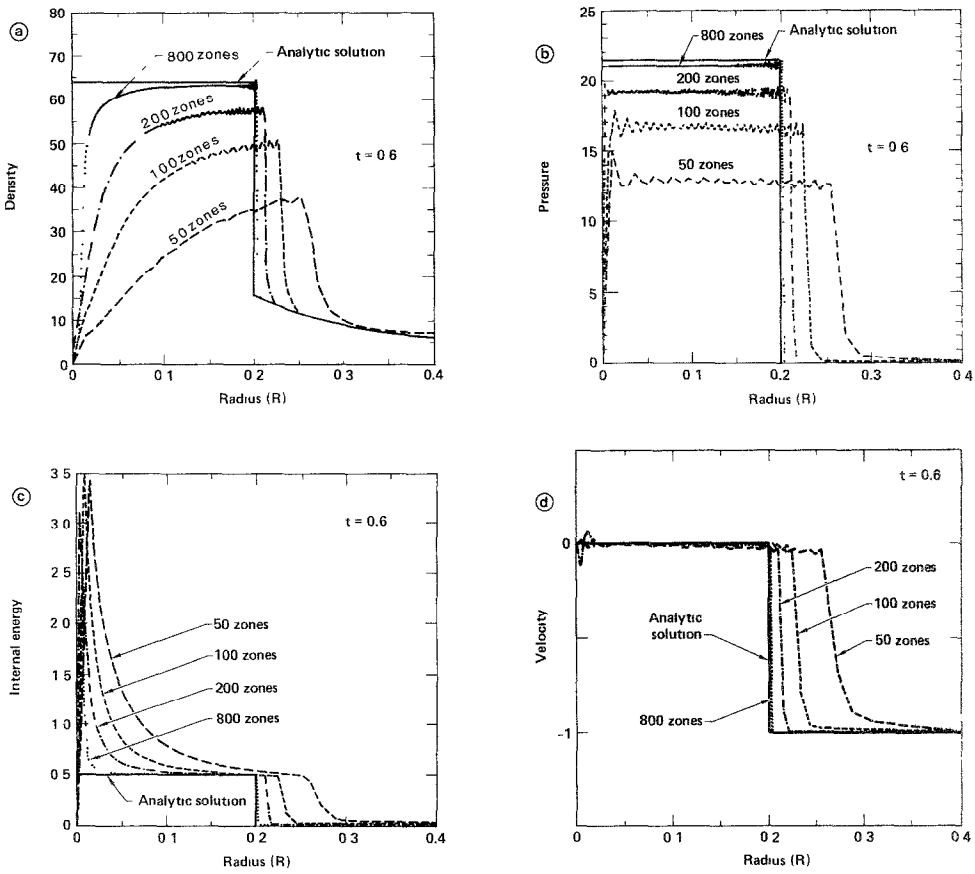

FIG. 19. (a) This example shows the truly large errors in density that result from using the **original** $Q_L(v) = 2(\Delta r)^2\ (r/R)^4\ (\Delta v/\Delta t)^2 = 2\rho[\Delta u + 2u\Delta R/R]^2$ (see (3.12)) for various mesh intervals (Δr). The comparisons are $t = 0.6$ and $\Delta r = 0.02$, 0.01, 0.005, and 0.00125, that is, for $K = 50$, 100, 200, and 800. This shows that the convergence of the density to the correct value $\rho^+ = 64$ is very slow indeed, and the error is unacceptable even for $K = 800$. (b) Likewise, the large errors in pressure for $K = 50$, 100, 200, and 800. The correct value is $P^+ = \frac{64}{3}$. (c) Errors in internal energy for $K = 50$, 100, 200, and 800. The exact solution is $\varepsilon^+ = \frac{1}{2}$. (d) This shows the very serious errors, using $Q_L(v)$, in the shock speed for the coarser grids of $K = 50$, $K = 100$, and even $K = 200$. Here, $S = \frac{1}{3}$ is the correct solution. (Figures 19a, b, c, and d are courtesy of M. P. Sohn of Los Alamos National Laboratory, who used one of Los Alamos' standard Lagrangian codes.)

associated with the shock smearing due to Q, which "senses" an incorrect (i.e., too small) jump-off value of the preshock density (ρ^-). That is, the Q shock smearing selects a $\rho^- < 16$. This error is a maximum at early times and becomes less serious in time as (the similarity) solution spreads out the preshock region over more and more mesh points, and thus the fixed shock thickness (i.e., it is always spread over $\simeq 3$ mesh points) becomes a smaller fraction of the preshock region. **The key to**

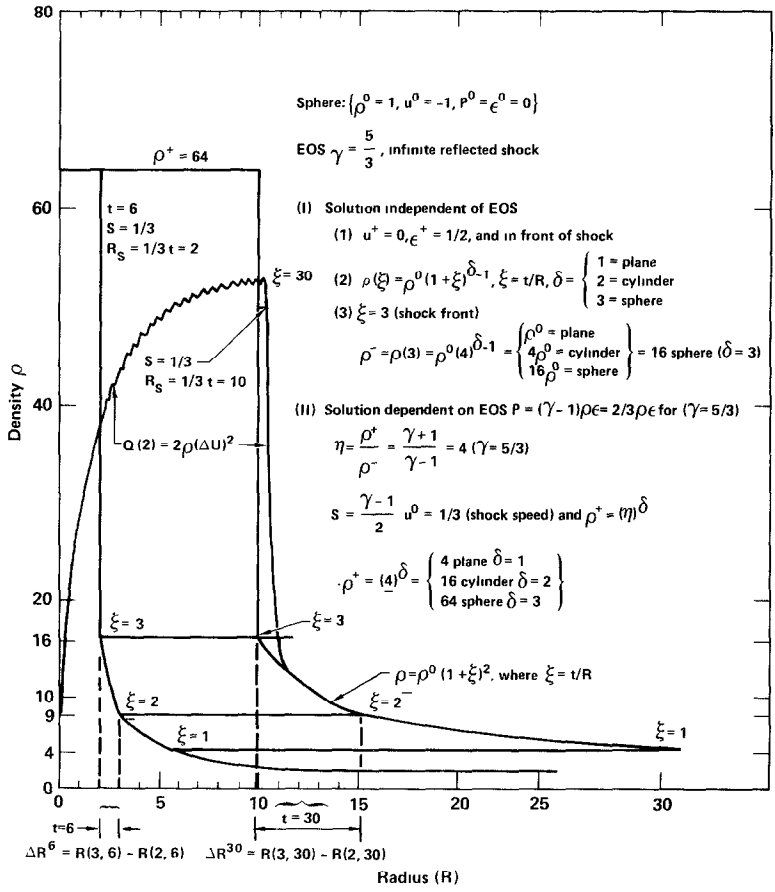

FIG. 20. The solution for Noh's spherical test problem (Fig. 17d) is given at two different times ($t = 6$ and $t = 30$) for the scale variable $\xi = t/R$. As t increases, the preshock density profile is spread over a physically greater and greater distance. Hence, the preshock value $\rho^- = 16$ should be progressively easier to resolve numerically as time advances. The wiggly line is the numerical solution using the **standard** $Q_L = 2\rho(\Delta u)^2$. The numerical error is so large ($10\% \leqslant \varepsilon \leqslant 600\%$) that it hardly resembles the **exact** solution, $\rho^+ = 64$.

more accuracy, then, is to sharpen shocks as much as possible. We confirm this argument in Fig. 21, where we prove numerically that this Q error is an error of the Q **shock-smearing** method, and is thus already an error in the **exact** solution of the **differential equations with** Q. The argument is the same as in Section 4, where we seek the limit solution as $\Delta r \to 0$ while holding l constant in $Q = (C_0 l)^2 \rho(\Delta u/\Delta r)^2$. We see that the difference solution has indeed converged. Thus, this third type of error is related to the Q formulation, but not to the particular difference equations.

One way to sharpen shocks, as we found before, is to use Noh's **(Q & H) shock-following method** ((2.1, (2.2), and (2.3)). This works because using a heat flux H is

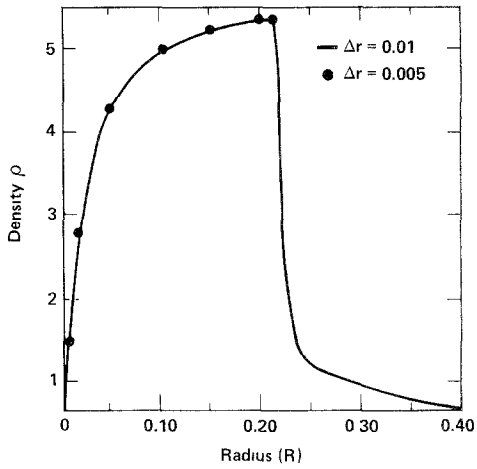

FIG. 21. Here we establish numerically (see Sections 4 and 8) that the difference solution (for $\Delta r = 0.01$) has essentially converged to the **exact** solution of the **differential equations** with $Q = (C_0 l)^2 \rho(u_r)^2$. We take $C_0^2 = 2$ and $l = 0.01$, and thus $Q = 2 \cdot 10^{-4} \rho(u_r)^2$. The solid curve is for $\Delta r = 0.01$ and $Q_L = 2 \cdot 10^{-4} \rho(\Delta u/\Delta r)^2 = 2\rho(\Delta u)^2$. Also, for $l = 0.01$, we let $\Delta r \to \Delta r/2 = 0.005$, giving $Q_L = 2 \cdot 10^{-4} \rho(\Delta u/\Delta r/2)^2 = 8\rho(\Delta u)^2$, which is plotted as dots (·), and we plot $R_k^n(\Delta r/2, \Delta t/2) = \frac{1}{2} R_k^n(\Delta r, \Delta t)$ (see discussion in Section 4.2). Thus, the spherical shock error is **not related** to the **difference method**, but is an error in the solution of the **differential equations** due to Q shock smearing.

conjunction with Q makes it possible to use smaller Q constants C_0^2 (and C_1) (while still keeping the noise level down behind the shock). This is shown in Fig. 22a, where the **standard** $Q_L(2) = 2\rho(\Delta u)^2$ is compared with the (Q_L & H_L) method using $Q_L(\frac{2}{3}, \frac{1}{5})$ and $H(4, 1)$. Using $Q_L(\frac{2}{3}, \frac{1}{5})$ gives sharper shocks and an improved value of ρ^+, and using the heat flux H smooths our the noise behind the shock. Of much more importance, however, is that the central heating error is nearly eliminated. This is seen in Fig. 22b, where $\varepsilon^+ \simeq \frac{1}{2}$ over the entire postshock region. Indeed, the results of Fig. 22, using (Q_L & H_L) would be nearly exact if one assumed that $\rho^- = 14.5$ (i.e., $\rho^+ = ((\gamma+1)/(\gamma-1))\rho^- = 4 \times 14.5 = 58$, and $u^+ = 0$, $\varepsilon^+ = \frac{1}{2}$, etc.), and thus the only real error in the calculated postshock values is due to the shock smearing that picks the wrong preshock density (i.e., $\rho^- \simeq 14.5$, as argued above). Just how the improvement goes with smaller Q constants C_0^2 and C_1 is shown in Fig. 23, where it is clear that the sharpest shock gives the most accurate solution.

In Fig. 24, the non-Q PPM of Colella and Woodward [7] produces very sharp shocks (on the order of one to two mesh widths). Here, they achieve high accuracy on the standard $K = 100$ test problem and nearly exact results using an accurate **adaptive-mesh shock-following procedure**, with $K = 400$. The $K = 400$ results are also shown to be nearly as accurate (converged) as the standard PPM solution with $K = 1200$. The effect of using an adaptive mesh is to minimize the actual (i.e., physical) shock thickness (which is all-important in determining the correct preshock value, $\rho^- = 16$, and it is thus clear that such a procedure would benefit any finite-difference method.

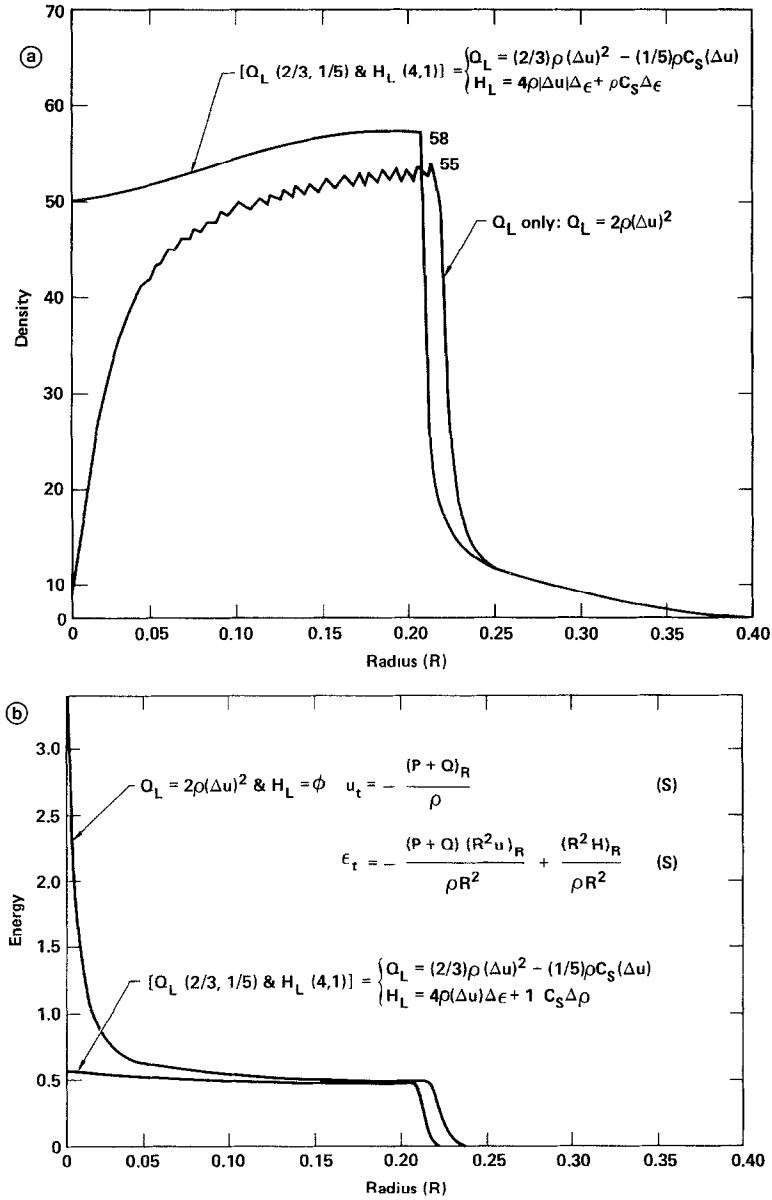

FIG. 22. (a) **Standard** $Q_L(2,0)=2\rho(\Delta u)^2$ vs $(Q_L \,\&\, H_L)$, where (using smaller Q_L constants C_0^2 and C_1 to give a sharper shock) $Q_L(\frac{2}{3},\frac{1}{5})=\frac{2}{3}\rho(\Delta u)^2-\frac{1}{5}\rho C_S(\Delta u)$ and $H_L(4,1)=4\rho|\Delta u|\Delta\varepsilon+\rho C_S\Delta\varepsilon$. The $(Q_L \,\&\, H_L)$ method is much smoother and more accurate than Q_L alone, but the error, $\Delta\rho^+=\rho^+-64$, is still on the order of 10 to 20%. (b) $Q_L=2\rho(\Delta u)^2$ and the more accurate $(Q_L \,\&\, H_L)$ method. The **exact** solution is $\varepsilon^+=\frac{1}{2}$, and we see that the energy error is essentially zero using the $(Q_L \,\&\, H_L)$ method. These results (Fig. 21) show that the error is due to the incorrect preshock density ρ^- and would be essentially exact if $\rho^-\simeq 14.5$. Then, in addition to the correct value $\varepsilon^+=\frac{1}{2}$, we would have $\rho^+=4\rho^-=4\times 14.5=58$, which is the observed value, and thus the Hugoniot jump conditions would be satisfied. The difficulty is seen to be that of shock smearing. That is, the correct value $\rho^-=16$ cannot be accurately resolved using $(\Delta r=0.01)$.

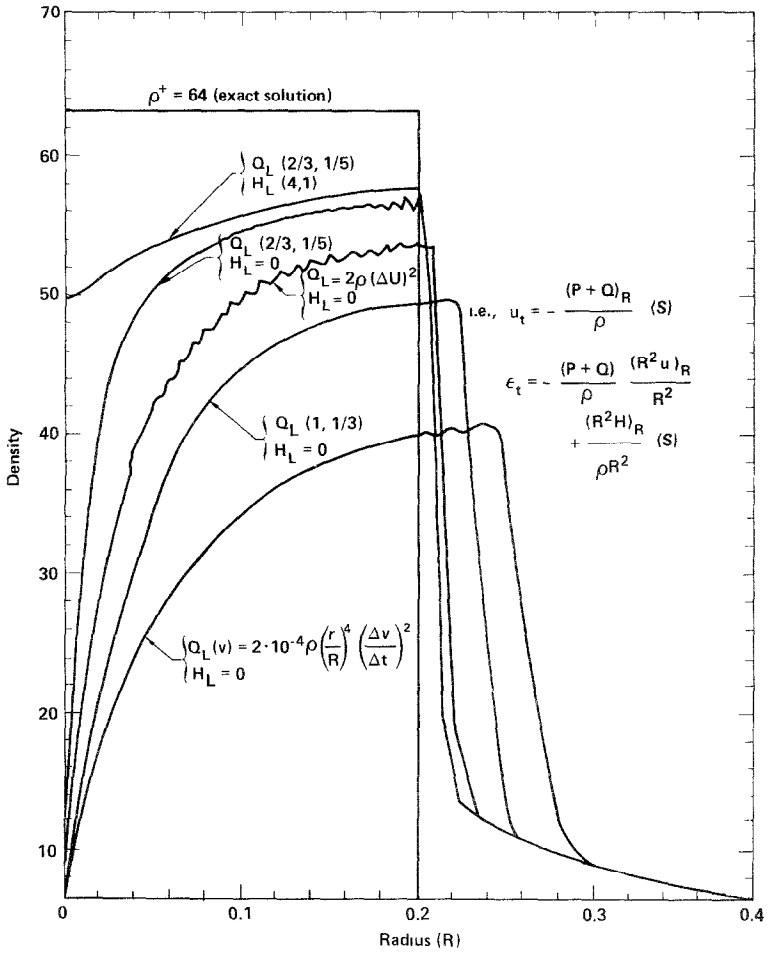

FIG. 23. Sharper shocks reduce the ρ^+ error. Errors go as $Q_L(1, \frac{1}{3}) > Q_L(2, 0) > Q_L(\frac{2}{3}, \frac{1}{5})$, where, in each case, there is less and less shock smearing. The $(Q_L \& H_L)$ method also allows for small Q coefficients, C_0 and C_1, and less central heating error to produce the sharpest shock profile.

9. SCALAR VERSUS SCHULZ'S TENSOR Q FORMULATIONS

In 1964, Schulz [8] proposed that Q be treated as a tensor viscosity and gave the following (T) formulation of the hydrodynamic equations (for $\delta = 1$, 2, and 3). We include the von Neumann–Richtmyer scalar (S) formulation, (2.1), again for comparison, and we note that use of the artificial heat flux, H, remains the same in both formulations:

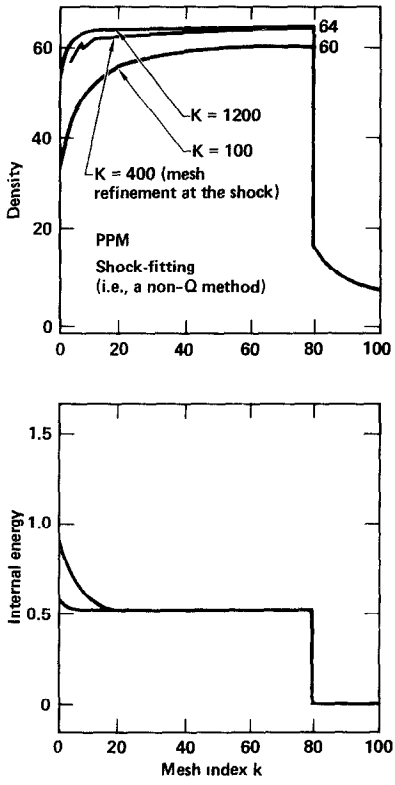

FIG. 24. The (non-Q) PPM of Colella and Woodward [7] has very narrow shocks ($\simeq 1$ or 2 mesh intervals) and for $K = 100$, is superior to all of the results of Fig. 23. PPM using $K = 400$ and mesh refinement (a shock-capturing adaptive mesh) is equivalent to the standard PPM using $K = 1200$ and is thus a very important procedure for tracking shocks accurately. (Figures courtesy of P. Woodward.)

$$\rho u_t + P_R = -Q_R$$
$$\rho(\varepsilon_t + Pv_t) = -Q\left[u_R + (\delta - 1)\frac{u}{R}\right] + \frac{1}{R^{\delta-1}}[R^{\delta-1}H]_R \qquad \text{Scalar (S)} \quad (9.1)$$

$$\rho u_t + P_R = -Q_R - \left[(\delta - 1)\frac{Q}{R}\right]$$
$$\rho(\varepsilon_t + Pv_t) = -Qu_R + \frac{1}{R^{\delta-1}}[R^{\delta-1}H]_R. \qquad \text{Tensor (T)} \quad (9.2)$$

Schulz also defined a new Q, which we denote by

$$Q_L(S) = C_0^2 \rho l^2 |u_{rr}|^{3/2} |u_r|^{1/2}, \qquad \text{if} \quad u_r < 0, \text{ and 0 otherwise.} \quad (9.3)$$

Here $l = \Delta r$ in the difference formulation as usual.

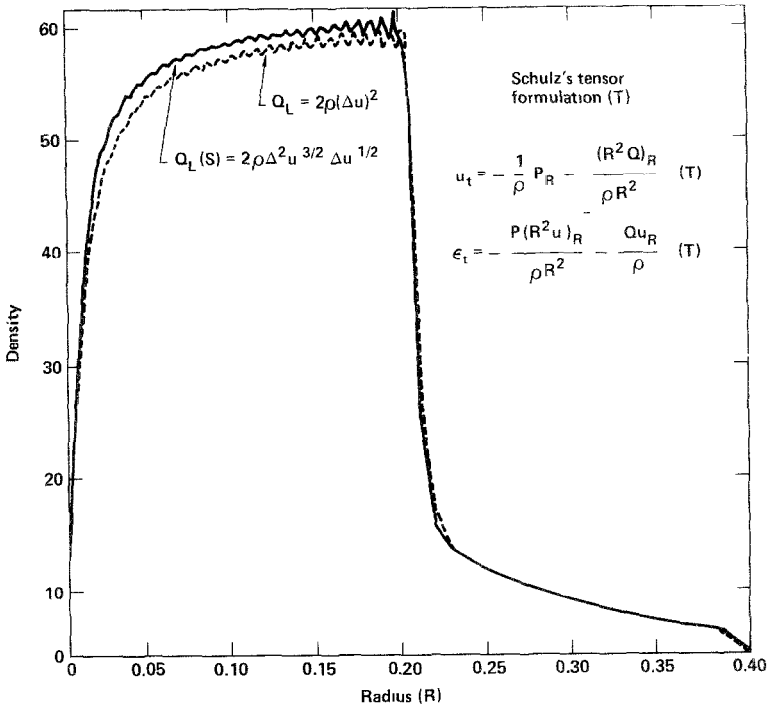

FIG. 25. The lower curve uses $Q_L(2, 0) = 2\rho(\Delta u)^2$ in Schulz's tensor (T) formulation (Section 9). The upper curve also uses Schulz's (T) formulation and, in addition, his $Q_L(S) = 2\rho|\Delta^2 u|^{3/2}\,|\Delta u|^{1/2}$. Both Q formulations are seen to give essentially the same results. We conclude that it is the tensor use of Q that is important rather than the Q_L formulation. Thus, we stay with the **standard** $Q_L = 2\rho(\Delta u)^2$ usage.

Now, Schulz's $Q_L(S)$ eliminates the **shockless** Q **heating** error (for the **uniform collapse** problem of Section 5—since $u_{rr} = 0$), and we thus might expect superior results for our spherical test problem 3. Indeed, the results (Fig. 25) using $Q_L(S)$ or Q_L with the tensor (T) formulation (9.2) are significantly better than using the scalar (S) equations (9.1), but there is essentially no improvement using $Q_L(S)$ over using Q_L. We conclude, then, that the major improvement occurs because of the way Q enters the equations, rather than the form of Q, and we stay with our **standard** $Q_L = C_0^2\rho(\Delta u)^2$. The reasons for the improved results are not entirely clear, but in part, the improvement follows from the formulation of (9.2), where there is **less** $Q\,dV$ **shock heating** than for the scalar equations (9.1). That is, in (9.2), $Q\,dv \to Qu_R$, independently of geometry ($\delta = 1$, 2, or 3), and thus the **nonshock** Q **heating term**, $Q(\delta - 1)u/R$, is eliminated from the energy equation.

In Fig. 26, we compare our **standard** $Q_L(2) = 2\rho(\Delta u)^2$ (T) with the (Q_L & H_L) (T) method (using $Q_L(2)$ and $H_L(6)$). The error in density is about the same just behind the shock, but the central heating error is nearly eliminated, as seen in Fig. 26b. To improve this result, it is necessary to narrow the shock width, and this

is done by reducing the Q_L constant C_0^2. In Fig. 27, we compare $Q_L(\frac{1}{4})$ (T) (which indeed has a narrower shock, but is extremely noisy) with ($Q_L(\frac{1}{4})$ and $H_L(10)$) (T) (which is still fairly noisy, but gives superior results).[7] These (Q_L & H_L) (T) results of Fig. 27 are reasonably smooth behind the shock and are essentially exact. Thus, we find the best all-around results for the 100-zone test problem are given by the (Q_L & H_L) **shock-following method** using Schulz's tensor formulations (9.2).

The results are summarized in Fig. 28, where we compare the various Q_L's, (Q_L & H_L), and the PPM.

10. Whalen's Tensor Q Formulation

Whalen, in Ref. 9 and in a private communication, presents some remarkably accurate results for our spherical test problem (see Figs. 29 and 30), which were obtained using his covariant tensor Q formulation of the hydrodynamic equations. We conclude by giving his formulations for $\delta = 1$, 2, or 3, and in particular, concentrate on the case of spherical geometry ($\delta = 3$),

$$\rho u_t (P + Q^R)_R = -(\delta - 1)(Q^R - Q^\phi)/R$$

and (10.1)

$$\rho \varepsilon_t + (P + Q^R) v_t = (\delta - 1)\, u(Q^R - Q^\phi)/R,$$

where Whalen defines

$$Q^R = (3/2)(C_0 l)^2 \rho (u_R - \tfrac{1}{3} \nabla \cdot \bar{u})$$

and (10.2)

$$Q^\phi = (3/2)(C_0 l)^2 \rho u_R (u/R - \tfrac{1}{3} \nabla \cdot \bar{u}),$$

and thus

$$Q^R - Q^\phi = \tfrac{3}{2}(C_0 l)\, \rho u_R^2 (u_R - u/R). \tag{10.3}$$

Now, let $\delta = 3$, then $\nabla \cdot \bar{u} = (u_R + 2u/R)$, and

$$Q^R = (C_0 l)^2 \rho u_R \left[u_R - \frac{u}{R} \right]. \tag{10.4}$$

Comparing (10.3) and (10.4), we see that

$$Q^R - Q^\phi = \tfrac{3}{2} Q^R, \tag{10.5}$$

[7] Subsequent tests show that the choice $C_0^2 = \frac{1}{3}$ and $h_0^2 = 10$ to be less noisy and essentially just as accurate as $C_0^2 = \frac{1}{4}$ and thus [$Q(\frac{1}{3})$ & $H(10)$] is to be preferred.

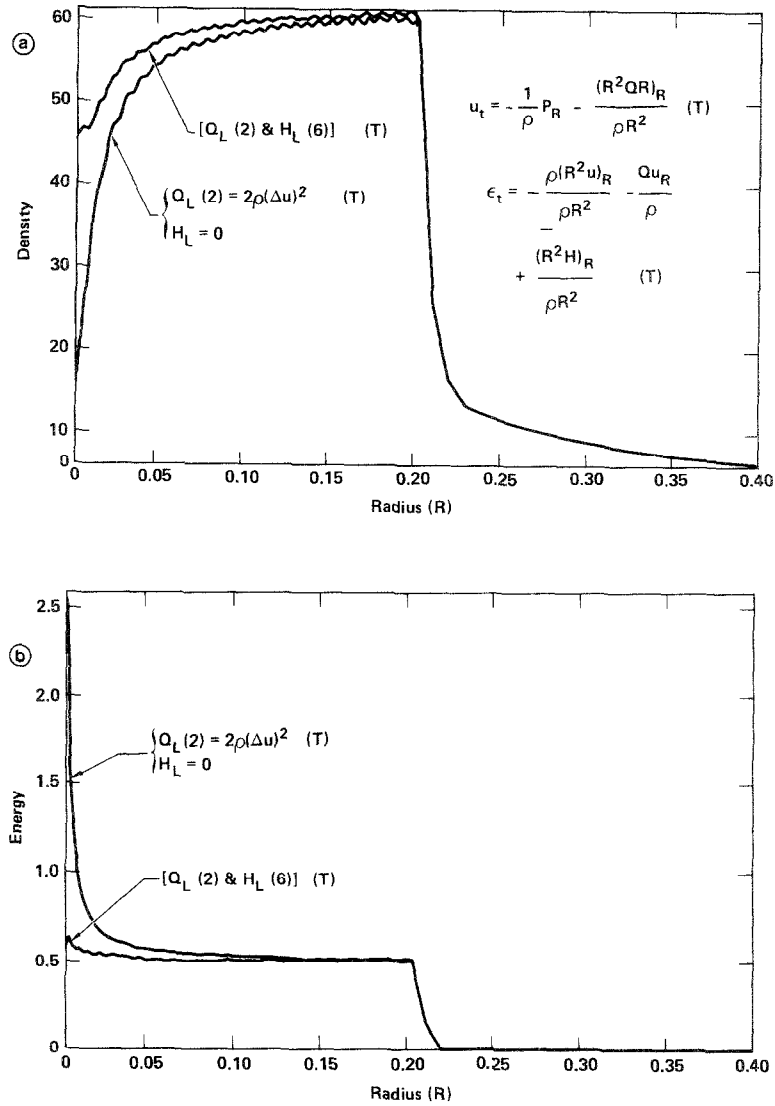

FIG. 26. (a) Schulz's tensor Q formulation with and without the use of an artificial heat flux H (see Section 9). The lower curve is the tensor (T) Q formulation using $Q_L = Q(2) = 2\rho(\Delta u)^2$ and $H \equiv 0$. The upper curve is $(Q_L \& H_L)$ (T) using $Q_L = 2\rho(\Delta u)^2$ and $H_L = 6\rho|\Delta u|\,\Delta\varepsilon$. This shows an obvious improvement using H_L with Q_L, but finer tuning is possible, as seen in Figs. 27a and b. (b) The overheating at the origin is greatly improved using $(Q_L \& H_L)$ (T), and in fact, is almost the exact solution, $\varepsilon^+ = \frac{1}{2}$.

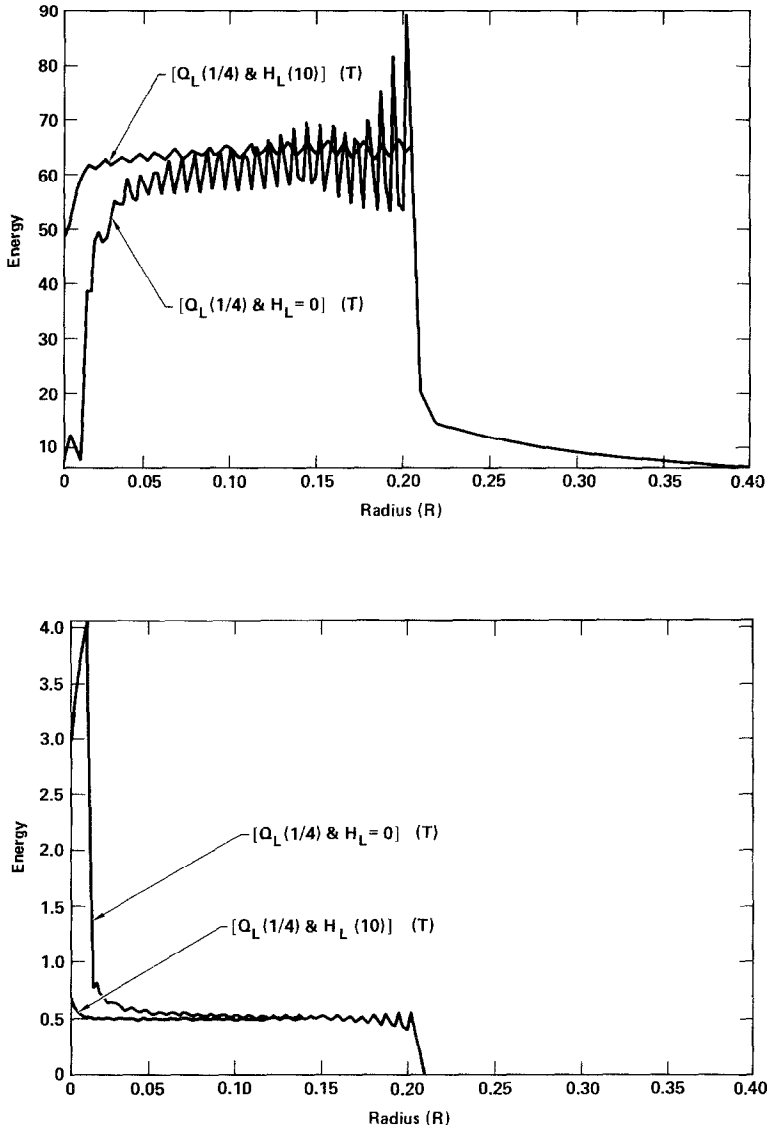

FIG. 27. $Q_L(\frac{1}{4}) = \frac{1}{4}\rho(\Delta u)^2$ in the (T) formulation is very noisy, but produces a narrow shock. (For more complicated problems, the choice $C_0^2 = \frac{1}{4}$ may be too small, as too much noise may be generated in the solution and thus reduce the computational Δt too severely. A more practical (but somewhat less accurate), all-around choice is $[Q_L(\frac{2}{3}, \frac{1}{5}) \& H_L(6, 0)]$ (T). That is, a more conservative use is $Q_L = \frac{2}{3}\rho(\Delta u)^2 - \frac{1}{5}\rho C_S \Delta u$ and $H_L = 6\rho|\Delta u|\,\Delta\varepsilon$, but $C_0^2 = \frac{1}{4}$ or $C_0^2 = \frac{1}{3}$ and $h_0^2 = 10$ are preferred where possible.) The sharp shock remains in the $[Q_L(\frac{1}{4}) \& H_L(10)]$ (T) method, where $H_L(10) = 10\rho|\Delta u|\,\Delta\varepsilon$, and most of the post-shock noise is damped. The density and energy errors are nearly zero; thus, the $(Q_L \& H_L)$ method is a preferred shock-following procedure when used with Schulz's tensor (T) formulation (9.2).

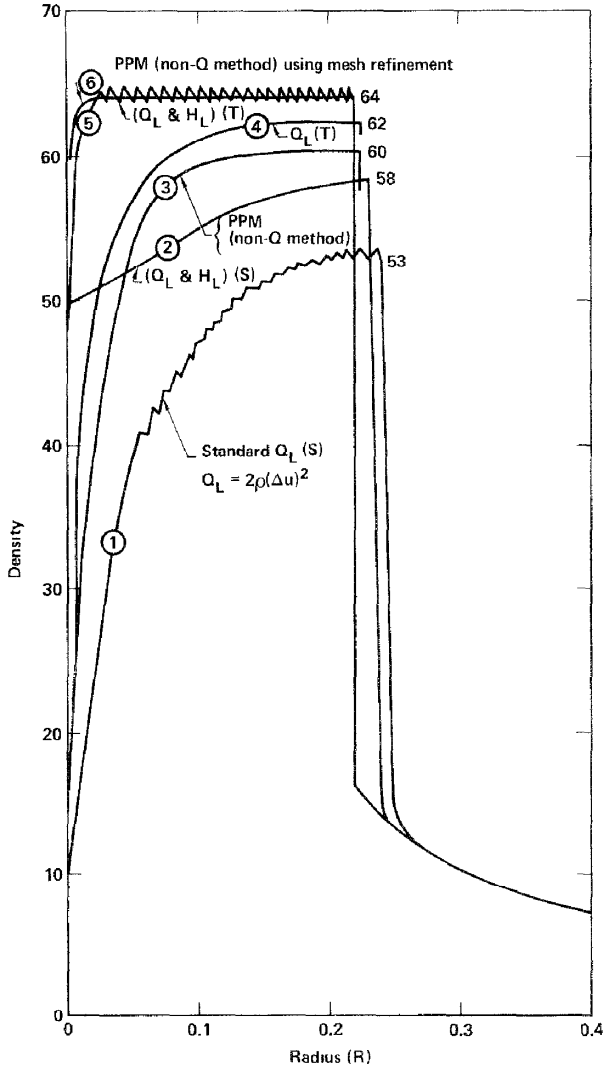

FIG. 28. A comparison of scalar (S) and tensor (T) results. The (non-Q) PPM lies above the best scalar (Q_L & H_L) (S) results, but is under the Q_L (T) and (Q_L & H_L) (T) results. The PPM [7] with mesh refinement and the (Q_L & H_L) (T) method give essentially the converged (**exact**) solution.

and we can write (10.1) (for $\delta = 3$) as

$$\rho u_t + (P + Q^R)_R = -3(Q^R)/R$$

and (10.6)

$$\rho \varepsilon_t + (P + Q^R)v_t = 3u(Q^R)/R.$$

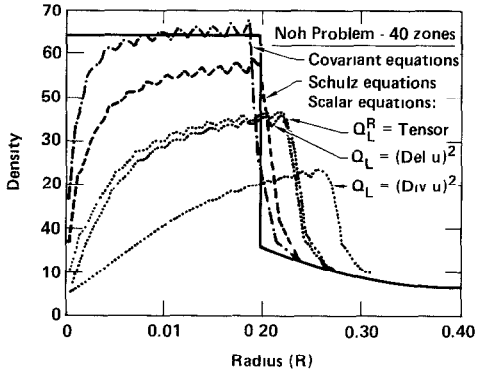

FIG. 29. Whalen's covariant formulation [9] (10.6) and (10.7), vs the scalar Q_L results and Schulz's tensor (T) formulation (Section 9). Here, Whalen defines $Q_L = (\text{Div } u)^2 = C_0^2\rho[\Delta u + 2u\Delta R/R]^2 = Q_L(v)$ (i.e., our (3.11)), $Q_L = (\text{Del } u)^2 = C_0^2\rho(\Delta u)^2 = Q_L$ (i.e., our (3.7)), and his tensor Q_L^R, $Q_L = C_0^2\rho(\Delta u)(\Delta u - u\Delta R/R)$. Whalen's formulation is remarkably accurate for a **40-zone** (K = 40) **problem.** (Figure courtesy of P. Whalen.)

In the difference formulation,[8] Whalen sets $l = \Delta R$, and thus

$$Q_L^R = C_0^2\rho\,\Delta u\left[\Delta u - \frac{u\,\Delta R}{R}\right] \text{ if } \Delta u \leqslant 0, \text{ and is otherwise 0.} \tag{10.7}$$

In Fig. 29, Whalen compares his covariant formulation (10.6) with Schultz's formulation (9.2) and the scalar equations (2.1) using various Q's. His notation means

$$Q = (\text{Div } u)^2 = Q_L(v) = C_0^2\rho\left[\Delta u + \frac{2u\,\Delta R}{R}\right]^2 \qquad \text{(i.e., our (3.11)];}$$

$$Q = (\text{Del } u)^2 = Q_L = C_0^2\rho(\Delta u)^2 \qquad \text{or our (3.7);}$$

and from (10.7),

$$Q_L^R(\text{tensor}) = C_0^2\rho(\Delta u)\left[\Delta u - \frac{u\,\Delta R}{R}\right].$$

Whalen's covariant results are clearly superior to the other Q formulations, and when we consider that only 40 zones ($K = 40$) are used in Fig. 29, then his formulation proves to be remarkably accurate. In Fig. 30, the effect of refined zoning is

[8] A word of caution: we were not able to reproduce Whalen's results with the most straightforward differencing of (10.6) and (10.7). In particular, (10.7) vanishes for the most central zone where $\Delta u = u$ and $\Delta R = R$ (i.e., $u\,\Delta R/R = (u/2)\,R/(R/2) = u$, and thus $\Delta u - u\,\Delta R/R = 0$]. In a like manner, Q_L^R also vanishes for our **uniform collapse** problem of Section 5, and this may contribute to his accurate results here. In any case, some subtlety is involved, and we await further clarification from Whalen on this subject.

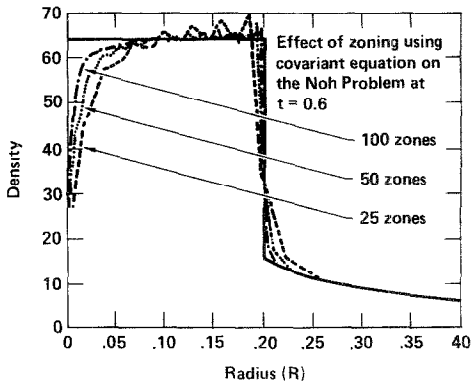

FIG. 30. Whalen's covariant tensor Q formulation, (10.6) and (10.7), where his tensor Q_L^R is given by $Q_L^R = C_0^2 \rho |\Delta u| [\Delta u - u\Delta R/R]$. The post-shock density is essentially correct ($\rho_{\text{exact}}^{+} = 64$), even for $K = 25$, and the convergence is considerably more accurate than for the scalar equations. (See Fig. 19 for a comparison of the effects of zoning on convergence.) (Figure courtesy of P. Whalen.)

shown for Whalen's covariant equations (10.6) and (10.7), and the results show a rapid convergence. Indeed, his results are remarkably accurate even for $K = 25$. Now, the type 1 (central, or wall heating) Q error is still present with this formulation (as it is for all Q formulations—see Section 4) and suggests that near-perfect results would be obtained bu including Noh's heat flux H in a $(Q_L^R \,\&\, H_L)$ shock-following method.

11. CONCLUSION

We conclude that the Q errors of types 1, 2, and 3 are not due to errors in any particular **difference-method** solution, but rather, the Q errors are intrinsic to the artificial-viscosity-Q shock following method itself. That is, these Q errors are contained in the **exact** solution to the **differential equation with** Q. Therefore, improvements must be sought in modifying the Q method itself (e.g., by using a tensor formulation or using both Q and H to follow shocks or to minimize the physical shock thickness, as in the non-Q PPM). More generally, since the Q errors are shown to be related to the (artificial) shock thickness of the shock-smearing procedure, then all methods will benefit from using an **adaptive-mesh** shock-capturing procedure. In all cases, narrow shocks produce the least error; thus the **$(Q_L \,\&\, H_L)$ shock-following method**, which allows the use of smaller Q constants—and thus sharper shocks—is to be preferred over Q alone; and **most important,** the inclusion of an artificial heat flux H **minimizes the excess** Q **heating** generated on shock reflection. In particular, it is shown that the $(Q_L \,\&\, H_L)$ method using Schulz's tensor (T) formulation (10.2) with minimal Q constants C_0^2 and C_1 is most satisfactory.

ACKNOWLEDGMENTS

I wish to thank John Hobson of LLNL for his invaluable help in implementing the various Q options tested here, particularly his efforts in testing the (Q & H) shock-following method. Also, except where noted otherwise, all of the splendid graphics are due to Hobson. Many thanks also to P. Woodward of LLNL and to P. Sohn and P. Whalen of Los Alamos National Laboratory for their contributions and helpful discussions in the spherical test problem comparisons for Sections 8 and 10.

REFERENCES

1. J. VON NEUMANN AND R. D. RICHTMYER, *J. Appl. Phys.* **21**, 232 (1950).
2. W. F. NOH, UCRL-89623, Lawrence Livermore National Laboratory, Livermore, CA, 1983 (unpublished).
3. R. D. RICHTMYER AND K. W. MORTON, *Interscience Tracts in Pure and Applied Mathematics*, (2nd ed.) (Interscience, New York, 1967).
4. J. F. TRULIO AND K. R. TRIGGER, UCRL-6267, Lawrence Livermore National Laboratory, Livermore, CA, 1961 (unpublished).
5. W. F. NOH, UCRL-7463, Lawrence Livermore National Laboratory, Livermore, CA, 1963 (unpublished).
6. J. WHITE, *J. Comput. Phys.* **12**, 553 (1973).
7. P. COLELLA AND P. WOODWARD, LBL-14661, Lawrence Berkeley Laboratory, Berkeley, CA, 1982 (unpublished).
8. W. D. SCHULZ, *J. Math. Phys.* **5**, 133 (1964).
9. P. P. WHALEN, Los Alamos National Laboratory Memo X-DO-PPW (3/84)-02, Los Alamos, NM, 1984 (unpublished).